TOWARD DETERMINING THE ROLE OF PKA IN CONTROLLING TORC2 FUNCTION AND CHEMOTAXIS IN *DICTYOSTELIUM DISCOIDEUM*

by

Alexandra Ruth Petlick

_____

A Thesis Submitted to the Faculty of the

DEPARTMENT OF CHEMISTRY AND BIOCHEMISTRY

In Partial Fulfillment of the Requirements

For the Degree of

MASTER OF SCIENCE
WITH A MAJOR IN CHEMISTRY

In the Graduate College

THE UNIVERSITY OF ARIZONA

2014

STATEMENT BY AUTHOR

This thesis has been submitted in partial fulfillment of requirements for an advanced degree at the University of Arizona and is deposited in the University Library to be made available to borrowers under rules of the Library.

Brief quotations from this thesis are allowable without special permission, provided that an accurate acknowledgement of the source is made. Requests for permission for extended quotation from or reproduction of this manuscript in whole or in part may be granted by the head of the major department or the Dean of the Graduate College when in his or her judgment the proposed use of the material is in the interests of scholarship. In all other instances, however, permission must be obtained from the author.

SIGNED: Alexandra Ruth Petlick

APPROVAL BY THESIS DIRECTOR

This thesis has been approved on the date shown below:

Pascale G. Charest
Assistant Professor of Chemistry and Biochemistry

May 7, 2014
Date

Acknowledgements

I would like to start by thanking Dr. Pascale Charest for her patience, kindness, and support over the past 3 years. I appreciate her enthusiasm and willingness to guide me as I made the transition from analytical chemistry to the more unfamiliar aspects of biochemistry. I've learned so much from her and I couldn't ask for a better PI.

Additionally, I extend my appreciation to my committee members, Dr. Craig Aspinwall and Dr. Michael Heien, for their support as both teachers and mentors. Their guidance and insight have been valuable as I faced the many challenges presented during these three short years of graduate school. I also want to thank Dr. Zachary Schultz, my undergraduate research advisor, for his continued support. Without him I wouldn't have even applied to U of A, and I am so thankful that I took his advice.

I am grateful for the camaraderie and friendship of all of the Charest lab members, especially Nieves Montaño for her kindness and encouragement as a colleague and friend. I'd also like to acknowledge Valery Thompson for her assistance in navigating all aspects of research from lab management to experimental protocols; undergraduate/rotation students Joe Cada, Maggie Scavello, and Nichole Eschleman for their eagerness to learn and their help with various aspects of the work presented here; Branden Stepanski for making history as the first male member of the "ladies-only" lab; and, finally, Tariq Islam, Shannon Collins, and Amanda Hanson, our newest members, for their humor and support. I wish you all the best!

Dr. Brooke Beam Massani has my thanks for all of the advice and knowledge she has provided since I first started working with her in the Keck facility. She taught me so much in the course of a year and helped me to rediscover my passion for microscopy, which has made an impact on my future ambitions. I also want to acknowledge Lori Boyd for her hard work and genuine concern for the well-being of students in the department, and for basically being a mom away from home.

I would like to acknowledge Rick Firtel for providing the Lifeact-GFP and GFP-Myo constructs, and Chris Janetopoulis for the spreadsheet used in chemotaxis calculations.

I also want to thank my friends, both in Tucson and around the world, for the laughter and the memories…grad school would have been intolerable if not for those meals and adventures shared outside of the lab. I am especially thankful for Dmitry; his love and positivity were an inspiration to me every step of the way.

Last, but certainly not least, I am forever grateful to my family for their love and never-ending encouragement. I want to thank Anna Petlick for her help in navigating Photoshop and C.J. Petlick (Dad) for his help in creating some of the figures presented in Chapter 3. I wouldn't have made it this far in life without my mom, Kris Petlick, and my youngest sister, Nellie Petlick, making me laugh and believing in me when it was difficult for me to believe in myself.

Table of Contents

Acknowledgements 3
List of Figures 6
Nomenclature & Abbreviations 10
Abstract 12
Chapter 1. Introduction and Motivation 13
Importance of TORC2 in Chemotaxis 18
Preliminary data 19
Chapter 2. Materials and Methods 23
2.1 Chemicals and Specialty Equipment 23
2.2 Molecular Biology (Kits, Enzymes, Cells, and Antibodies) 24
2.3 Primers and Oligonucleotides 25
2.4 Cell Culture 27
2.4.1 Growth and Maintenance of Cell Lines 27
2.4.2 Transformation of Dicty cells by Electroporation 27
2.5 Pulsing Dictyostelium cells with cAMP 28
2.6 Molecular Cloning 29
2.6.1 Amplification and Isolation of Insert DNA (PCR) 29
2.6.2 Digestion of Plasmid and Insert DNA 29
2.6.3 Transformation of Competent Bacteria (adapted from Nieves Montaño) 33
2.6.4 Picking Colonies 33
2.6.5 DNA Precipitation (for transformation of Dictyostelium) 34
2.6.6 Site-Directed Mutagenesis 34
2.7 Protein Manipulations 36
2.7.1 Protein Quantification 36
2.7.2 SDS-PAGE Gels 36
2.7.3 Gel Transfer 36
2.7.4 Blocking and Antibody Incubation 37
2.7.5 Imaging 37
2.7.6 Coomassie Staining 37
2.8 Microscopy 38
2.8.1 Imaging System 38

2.8.2 Chemotaxis Assays 38
2.8.3 Random Motility Assays 39
2.8.4 Uniform Stimulation Assays 40
2.8.5 Cell Tracking 40
2.8.6 Quantification of Fluorescence Intensity 41
Chapter 3. Results and Discussion 42
3.1 Characterization of Chemotaxis Phenotype 42
3.1.1 Results 42
3.2.2 Discussion 49
3.2 F-Actin Dynamics 55
3.2.1 Results 55
3.2.2 Discussion 59
3.3 Myosin II Dynamics 61
3.3.1 Results 61
3.3.2 Discussion 63
3.4 Actin/Myosin Dual Reporter Construct 66
3.4.1 Results 66
3.4.2 Discussion 67
3.5 RBD-GFP Assays 70
3.5.1 Introduction 70
3.5.2 Results 70
3.5.3 Discussion 72
3.6 Rap1 Phosphorylation Mutants 73
Chapter 4. Conclusions and Future Directions 75
References 78

List of Figures

Figure 1.1. Aggregation of *Dictyostelium discoideum* via cAMP signal relay. Starved cells begin to produce and secrete cAMP as a signal to aggregate. Neighboring cells detect this signal and use the gradient to migrate toward the aggregation center while relaying the signal to cells further away. (courtesy of Branden Stepanski)……..p. 14

Figure 1.2. Molecular structure of cAMP (cyclic adenosine monophosphate), the key chemoattractant in *Dictyostelium discoideum*……..p. 14

Figure 1.3. F-actin polymerization and Myosin II contraction work in tandem to produce cellular translocation. In a resting cell, signaling molecules and cytoskeletal proteins are homogenously distributed within the cytoplasm. Upon sensing of a chemoattractant gradient, the cytoskeleton rearranges with F-actin at the front and assembled Myosin II at the sides and rear, enabling the cell to perform chemotaxis. ……..p. 16

Figure 1.4. Signaling proteins and cytoskeletal components are localized and regulated in polarized cells. Proteins involved in detecting cAMP and relaying the signal to downstream effectors of chemotaxis are localized at the front of a polarized cell. Key components of the signaling cascade that are considered in this study include active Ras/Rap1 and TORC2. These proteins are linked to localization and assembly of F-actin and myosin II at the front and rear of the cell, respectively. Figure adapted from Sasaki & Firtel, 2006.[15]……..p. 16

Figure 1.5. RasC-TORC2-PKB/PKBR1 pathway. Note PKA (in yellow), the protein of interest in this study. The research presented in this thesis aims to improve understanding of the role of PKA in regulating TORC2 activity and, thus, chemotactic responses. ……..p. 17

Figure 1.6. PKA holoenzyme showing regulatory and catalytic subunits and activation by cAMP. PKA is activated upon binding of cAMP to receptors on the regulatory subunit dimer. This prompts dissociation and release of the catalytic subunits, which are then free to phosphorylate other proteins……p. 17

Figure 1.7. PKA-mediated negative feedback regulation of Rap1 and TORC2. **A.** Chemoattractant-induced Rap1 activity is elevated and extended in cells lacking TORC2 or PKA. Cells lacking PKA activity [pkaC null, acaA null, or treated with the PKA inhibitor H89 (PKA-I)] also display elevated TORC2 activity (**B**), PKB activity (**C**), and Sca1 phosphorylation (**D**), but reduced Sca1 membrane localization (**E**) and RasC activity (**F**). (courtesy of Pascale Charest) ……p. 20

Figure 1.8. PKA regulates TORC2 activity. TORC2 activity is elevated and extended in cells with constitutive PKA activity. This assay detects phosphorylation of PKB/PKBR1 HM (hydrophobic motif) which is mediated by TORC2, thus providing a measure of TORC2 activity……p.20

Figure 1.9. A conceptual model of the proposed mechanism for regulation of Rap1 by PKA. This model illustrates the possible inhibition of Rap1 by PKA, leading to lowered TORC2 activity and misregulation of downstream cytoskeletal proteins (including Myosin II and F-actin). (courtesy of Pascale Charest)……p.22

Figure 2.1. Vector map for extrachromosomal expression vector pDM304.[24] (Image from DictyBase; http://dictybase.org/data/plasmid/images/532.jpg).[25]……p. 30

Figure 2.2. Vector map for shuttle vector pDM328, containing N-terminal mRPFmars tag.[24] (Image from DictyBase;
http://dictybase.org/data/plasmid/images/553.jpg).[25]……p. 31

Figure 2.3. Vector map for integrating expression vector pEXP4(+).[26,27] (Image from DictyBase; http://dictybase.org/data/plasmid/images/356.jpg).[25]……p. 32

Table 3.1. Statistics for random motility of vegetative cells. Cellular movement was analyzed during three different 30-minute periods after the onset of starvation. Persistence is a measure of path linearity calculated as total linear displacement divided by the total distance traveled. No statistical difference was observed in persistence between cell lines. Distance and speed measurements are illustrated graphically in Figure 3.1. The data above was compiled from 191 individual cell traces……p. 43

Figure 3.1.A. Non-linear distance moved by vegetative AX3 (◆), *pkaC*- (▲), and *pkaR*- (■) cells as a function of starvation time over the course of a time lapse series. **B.** Speed of vegetative cells at consecutive time points after onset of starvation. Speed is reported as an average of instantaneous speed values obtained by manual tracking of a time lapse series. Each data point represents an average of multiple experiments. Error bars indicate the standard deviation of compiled data for each point.p. 43

Figure 3.2. Morphology of cell lines studied. Cells pictured were imaged in DIC mode after at least 10 minutes within an established gradient of cAMP and are representative of several experiments……p. 44

Figure 3.3. Cell traces aligned along a straight path from start position along the cAMP gradient. Black circles indicate the endpoints of traced paths. Traces are aligned with all starting points at the origin of two perpendicular lines and the start and end points positioned relative to a straight line along the cAMP gradient. ……p. 47

Table 3.2. Statistics for chemotaxis of starved cells. Motility speed is an average of instantaneous speeds along a path, migration speed is total linear displacement over time, and persistence is a measure of path linearity. Chemotactic index is a fractional indicator of cell movement along the cAMP gradient. Sample sizes: AX3, 10 samples; *pkaC*-, 8 samples; *pkaR*-, 8 samples. ……p. 47

Figure 3.4. Geometric determination of chemotactic index. **S** represents the cell's starting position, **E** represents its ending position, and **N** indicates the location of the micropipette (needle) diffusing cAMP. Φ is the angle between the straight line vector from the cell's start position to the needle (*A*) and the straight line vector from the cell's start to end position (*B*). ……p. 48

Figure 3.5. Comparison of two different stocks of AX3 cells used in experiments. Images were collected after 30 minutes of exposure to a cAMP gradient. Note that the old stock of cells (left) fail to polarize whereas cells in the new stock obtained from DictyBase (right) elongate and perform chemotaxis more efficiently. ……p. 54

Figure 3.6.A. Response of AX3 cells containing an F-actin reporter to uniform cAMP stimulation. Cells were monitored via confocal fluorescence microscopy over a period of 60 seconds to record their response. F-actin polymerization at the plasma membrane is apparent within 3 seconds after uniform stimulation. **B.** Quantification of membrane-localized Lifeact-GFP (actin reporter) as a function of time. All data was normalized to the basal level of fluorescence at T=0, reflecting an increase and subsequent decrease in membrane-localized Lifeact-GFP after stimulation. Sample sizes: AX3, 70 samples; *pkaC-*, 47 samples; *pkaR-*, 87 samples. ……..p. 57

Figure 3.7. F-actin (Lifeact-GFP) localization in chemotaxing cells. The fluorescent reporter indicates enrichment of F-actin at the leading edge of AX3 cells moving in the direction of a cAMP gradient. Both *pkaC-* and *pkaR-* cells display localized F-actin at membrane protrusions when exposed to the same chemoattractant gradient despite their reduced ability to polarize and migrate efficiently; however, this polymerization of F-actin is not confined to the front—especially for *pkaC-* cells—toward the highest concentration of chemoattractant. ……..p. 60

Figure 3.8.A. Response of AX3 cells containing GFP-Myosin to uniform cAMP stimulation. Initially, a low level of cortex-localized GFP-Myosin can be observed. Upon stimulation, GFP-Myosin is delocalized from the cell cortex and moves to the cytosol before it translocates back to the cortex, with a peak around 30 seconds, and goes back to basal levels by 60 seconds after stimulation. **B.** Quantification of membrane-localized GFP-Myosin as a function of time. Sample sizes: AX3, 61 samples; *pkaC-*, 28 samples; *pkaR-*, 54 samples. ……..p. 62

Figure 3.9. GFP-Myosin in chemotaxing cells. The fluorescent reporter indicates assembly of Myosin II at the sides and posterior of AX3 cells chemotaxing in a cAMP gradient. Both *pkaC-* and *pkaR-* cells display localized GFP-Myosin when exposed to the same chemoattractant gradient despite their reduced ability to polarize and migrate efficiently. Note that localization of GFP-Myosin in the *pkaC-* cells pictured is oriented on the edge closest to the source of the chemoattractant. This is due to the cells migrating away from (instead of toward) the gradient—further highlighting their chemotactic deficiencies. GFP-Myosin is represented as pseudocolor red. ……..p. 65

Figure 3.10. Sequence for forward oligonucleotide used to amplify *mhcA* (Myosin). The sequence begins with a 5-nucleotide sequence to initiate annealing and anchor the primer. This is followed by the 6-nucleotide sequence for BamHI to introduce a restriction site for cloning. Next, the sequence for a linker (GGSG) is inserted to permit flexibility upon fusion of Myosin and mRFP. Finally, the first 28 nucleotides in the *mhcA* sequence are included to initiate amplification of the gene……..p. 68

Figure 3.11. Cloning strategy for LifeactGFP/RFP-Myosin in pDM304. Lifeact-GFP was cloned into the BglII/SpeI double-digest restriction site of vector pDM304. Myosin was then amplified via PCR and cloned into the BglII/SpeI double-digest restriction site of shuttle vector pDM328 containing the sequence for mRFPmars. The resulting plasmid was then digested with NgoMIV to remove the cassette containing mRFPmars-Myosin; this was then cloned into the NgoMIV restriction site in the Lifeact-GFP/pDM304 construct. ……..p. 68

Figure 3.12. Investigating the spatiotemporal dynamics of F-actin and RFP-Myosin in wild-type cells using the tandem-expression construct Lifeact-GFP/RPF-Myosin/pDM304. F-actin is enriched at the leading edge as anticipated, whereas Myosin II is not enriched at the sides and rear of the chemotaxing cell. ……..p. 69

Figure 3.13.A. Response of AX3 cells containing GFP-RBD to uniform cAMP stimulation. Localization of the reporter at the membrane peaks at 5 seconds after stimulation of starved cells with cAMP.
B. Relative to AX3 cells, both PKA mutants take slightly longer to respond to the stimulus and also display reduced levels of Ras activation. Sample sizes: AX3, 20 samples; *pkaC-*, 9 samples; *pkaR-*, 32 samples…….p. 71

Figure 4.1. Key pathways implicated in chemoattractant signal transduction in Dictyostelium. The chemoattractant (cAMP) receptor cAR1 and downstream heterotrimeric G protein promote the activation of many downstream signaling pathways, in which Ras family GTPases play a central role. Further work needs to be done to address the potential cross-talk of RasC and Rap1 pathways through TORC2. (courtesy of Pascale Charest) ……p. 76

Nomenclature & Abbreviations

aa	Amino acid
ACA	Adenylyl cyclase A
Amp	Ampicillin
APS	Ammonium persulfate
ATP	Adenosine triphosphate
bp	Base pairs
BSA	Bovine serum albumin
cAMP	Cyclic adenosine monophosphate
Dicty	*Dictyostelium discoideum*
DNA	Deoxyribonucleic acid
DMSO	Dimethyl sulfoxide
DTT	Dithiothreitol
dNTP	Deoxyribonucleotide triphosphate
EDTA	Ethylenediaminetetraacetic acid
EtOH	Ethanol
G418	Geneticin
GFP	Green fluorescent protein
GPCR	G-protein coupled receptor
GTP	Guanosine-5'-triphosphate
hr(s)	Hour(s)
kb	Kilobase pairs
kDa	kilodaltons
L	liter
LB	Lysogeny broth
M	Molarity (moles/L)
mA	Milliamps (10^{-3} amps)
MeOH	Methanol
mhcA	Myosin heavy chain A
min(s)	Minute(s)
mM	Millimolar (10^{-3} moles/L)
mm	Millimeter (10^{-3} meter)
ms	Milliseconds (10^{-3} seconds)
MW	Molecular weight
Myo	Myosin
nm	Nanometer (10^{-9} meter)
ng	Nanograms (10^{-9} grams)
oligo	Oligonucleotide
O/N	Overnight
PCR	Polymerase chain reaction
PKA	Protein kinase A

RA	Ras/Rap association domain
RBD	Ras binding domain
RFP	Red fluorescent protein
RPM	Revolutions per minute
RT	Room temperature (roughly 22°C)
SDS	Sodium dodecyl sulfate
sec(s)	seconds
TBS	Tris buffered saline solution
TBST	Tris buffered saline/Tween solution
TEMED	Tetramethylethylenediamine
T_m	Melting temperature
TORC2	Target of rapamycin 2
Tris	Tris(hydroxymethyl)aminomethane
Tween	Polysorbate 20
V	Volt
WT	Wild-type
µg	microgram (10^{-6} grams)
µL	microliter (10^{-6} liters)
µM	micromolar (10^{-6} moles/L)
µm	micrometer/micron (10^{-6} meters)

Abstract

Chemotaxis is a process whereby single- and multi-cellular organisms migrate in response to external chemical stimuli. This directed cell movement is regulated by complex signaling pathways and is implicated in embryonic development, immune response, and the metastasis of cancer cells. *Dictyostelium discoideum*, social amoebae with the ability to migrate and aggregate in response to chemoattractants such as cAMP, have been used as a model system to study chemotaxis. Preliminary research suggests that protein kinase (PKA) is involved in some of the signaling pathways that regulate chemotaxis. The role of PKA in chemotaxis was investigated, first, by characterizing the phenotype of PKA null cells using established cell biological and biochemical assays. Furthermore, spatiotemporal regulation of critical cytoskeletal proteins was probed in wild-type and PKA null cells using confocal fluorescence microscopy, indicating misregulation of both F-actin and Myosin II in *pkaC*- and *pkaR*- cells. Finally, preliminary work was done to lay the groundwork for experiments exploring possible PKA targets mediating TORC2 function in chemotaxis.

Chapter 1. Introduction and Motivation

Chemotaxis, or directed cell migration, toward a chemical signal (chemoattractant) is critical for many biological processes. This chemoattractant detection and cell movement is essential for tissue formation during embryonic development, inflammatory responses and wound healing, interstitial leukocyte trafficking, and cancer metastasis.[1–7]

Complex signaling pathways are instrumental in allowing cells to sense the direction of a chemoattractant gradient, process and propagate the signal, and initiate movement toward the source of the chemoattractant. Our group seeks to better understand the intracellular regulatory pathways that direct chemotaxis. We use *Dictyostelium discoideum*, a species of soil-living amoeba, as a model system to explore the mechanisms behind chemotaxis. These organisms are ideal for the study of chemotaxis as the signaling pathways are highly conserved from *Dictyostelium* to mammalian cells.[8–10] Additionally, *Dictyostelium* are easy to grow and their genes are easily manipulated through homologous recombination, making biochemical and cell biological analyses more accessible than in higher organisms.[11,12]

In their natural habitat, *Dictyostelium* live primarily as single-cell organisms but aggregate to form multicellular structures when challenged by starvation or otherwise unfavorable conditions. Figure 1.1a. shows a schematic representation of cellular aggregation by propagation of a cAMP signal. Cells begin to secrete cAMP which acts as a chemical signal to rally other cells to aggregate.[13] Detection of a cAMP gradient is regulated by G-protein-coupled receptors (GPCRs), specifically the cAMP receptor 1 (cAR1). The GPCR then activates signaling

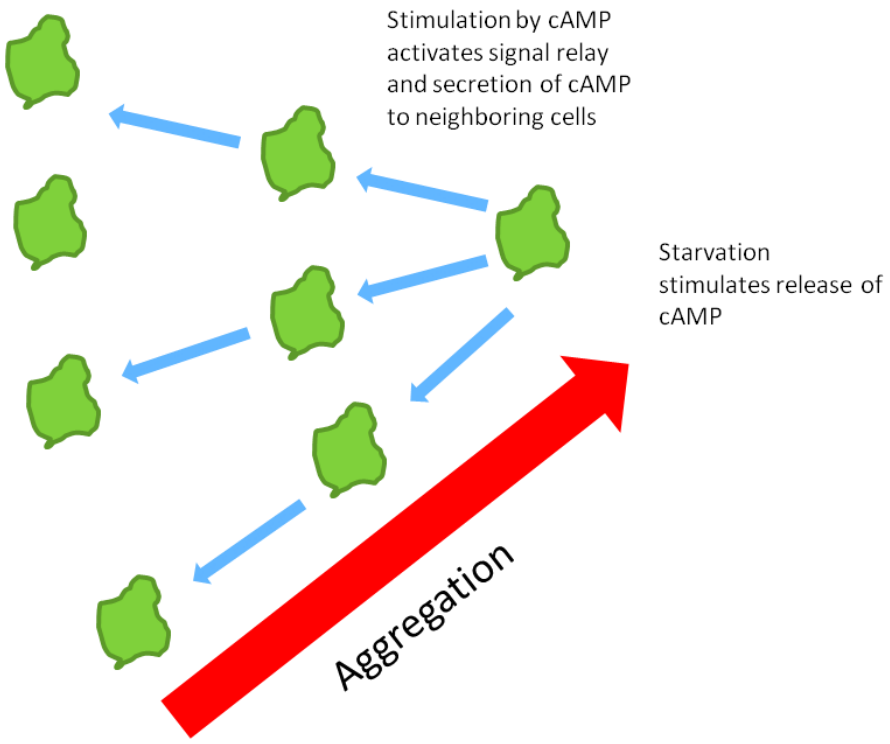

Figure 1.1. Aggregation of *Dictyostelium discoideum* via cAMP signal relay. Starved cells begin to produce and secrete cAMP as a signal to aggregate. Neighboring cells detect this signal and use the gradient to migrate toward the aggregation center while relaying the signal to cells further away. (courtesy of Branden Stepanski)

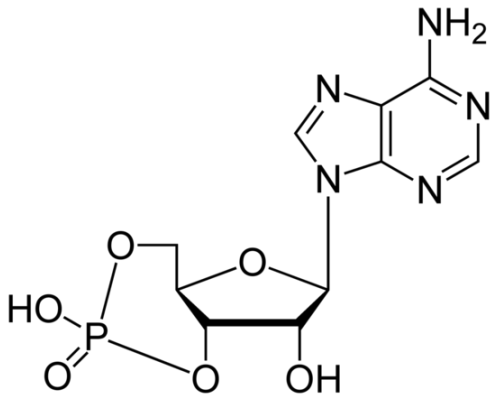

Figure 1.2. Molecular structure of cAMP (cyclic adenosine monophosphate), the key chemoattractant in *Dictyostelium discoideum*.

cascades which result in cellular responses and propagation of the chemical signal by synthesis of cAMP via adenylate cyclase A (ACA) and subsequent cAMP secretion.[14]

Upon detection of a chemoattractant gradient, *Dictyostelium* polarize and orient themselves to move toward the aggregation center from which the signal is emanating. At rest, cells contain a random distribution of signaling and cytoskeletal molecules. Upon polarization, chemotaxis can be achieved due to organization and cooperativity of polymerized filamentous actin (F-actin) and assembled Myosin II. Figure 1.2 illustrates cytoskeletal reorganization upon detection of a chemoattractant gradient with F-actin enriched at the leading edge and Myosin II localized at the rear of the cell. In order to move forward toward a chemoattractant, a protrusion (or pseudopod) develops at the front of the cell due to polymerization of F-actin. Simultaneously, the rear of the cell moves forward due to contraction of the Myosin II-containing cytoskeleton. In the presence of a chemoattractant gradient, directed movement toward the source is a result of receptors distributed around the cell perimeter which initiate the signaling pathways controlling myosin and actin. As shown in Figure 1.3, various proteins implicated in the chemotaxis signaling pathway also localize to the front, back, and sides of the cell to facilitate a directional migration and signal relay.

As shown in Figure 1.4, the pathways controlling chemotaxis are highly complex and interlaced. Many interactions in the pathway have been proposed but have yet to be confirmed or clarified, indicated by dashed lines.

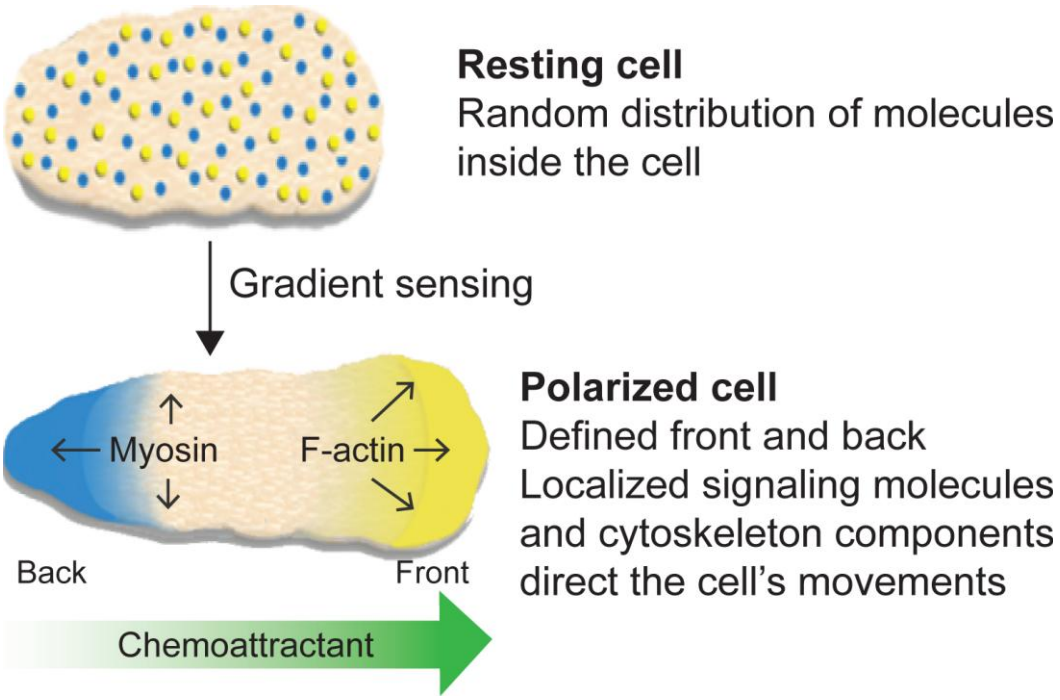

Figure 1.3. F-actin polymerization and Myosin II contraction work in tandem to produce cellular translocation. In a resting cell, signaling molecules and cytoskeletal proteins are homogenously distributed within the cytoplasm. Upon sensing of a chemoattractant gradient, the cytoskeleton rearranges with F-actin at the front and assembled Myosin II at the sides and rear, enabling the cell to perform chemotaxis.

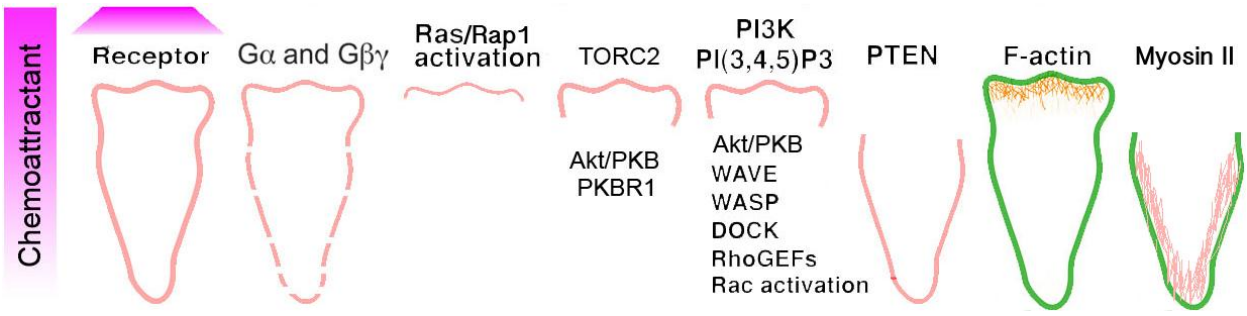

Figure 1.4. Signaling proteins and cytoskeletal components are localized and regulated in polarized cells. Proteins involved in detecting cAMP and relaying the signal to downstream effectors of chemotaxis are localized at the front of a polarized cell. Key components of the signaling cascade that are considered in this study include active Ras/Rap1 and TORC2. These proteins are linked to localization and assembly of F-actin and myosin II at the front and rear of the cell, respectively. Figure adapted from Sasaki & Firtel, 2006.[15]

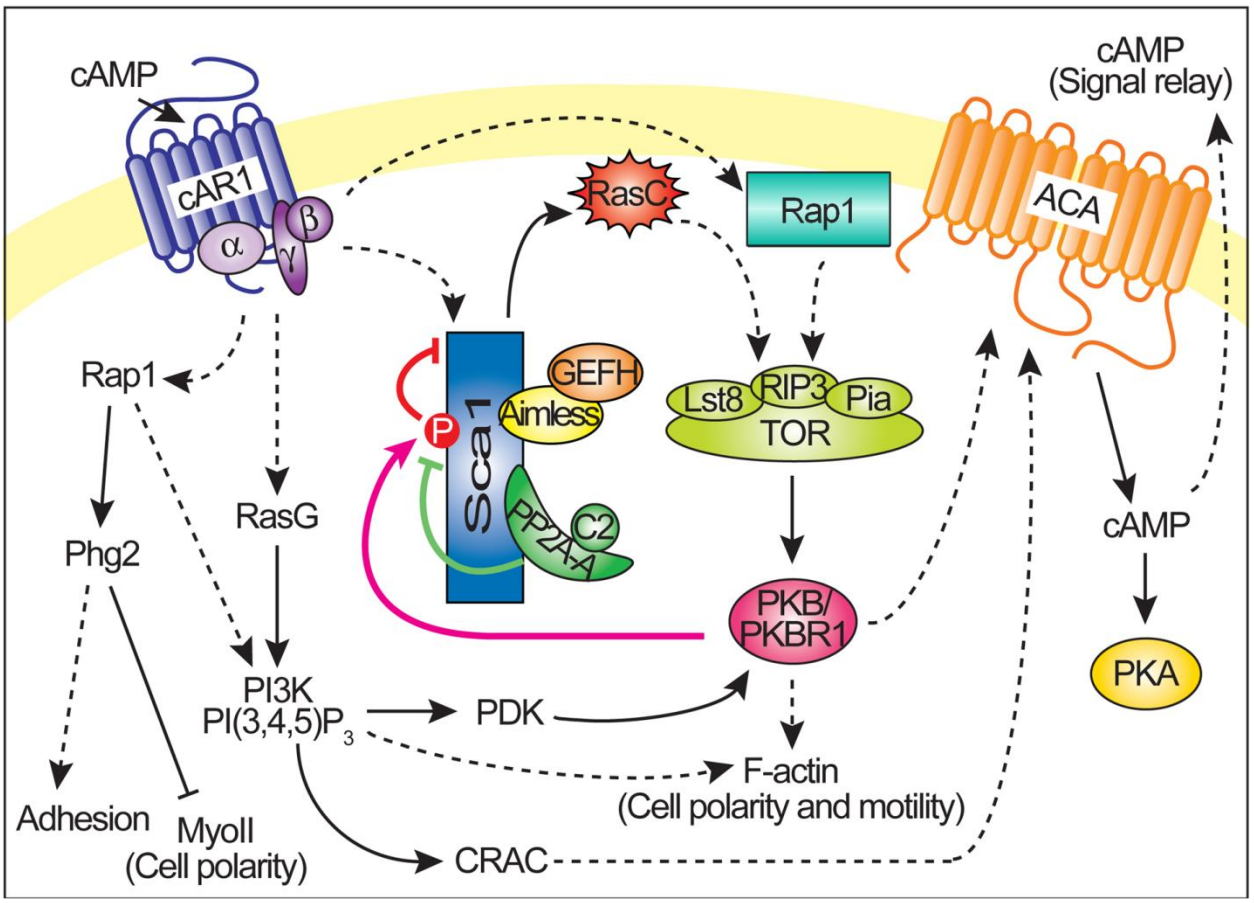

Figure 1.5. RasC-TORC2-PKB/PKBR1 pathway. Note PKA (in yellow), the protein of interest in this study. The research presented in this thesis aims to improve understanding of the role of PKA in regulating TORC2 activity and, thus, chemotactic responses.

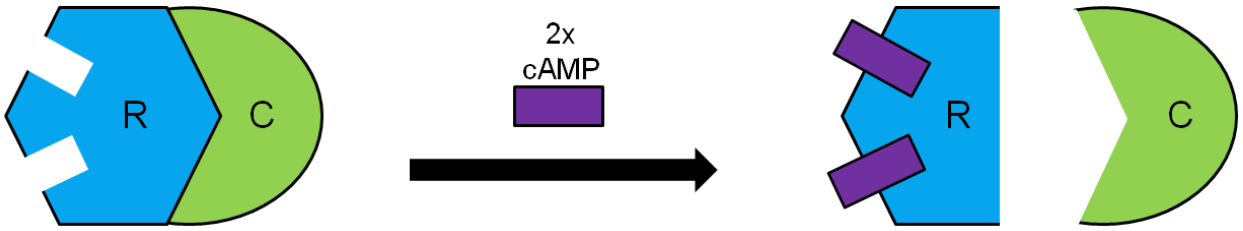

Figure 1.6. PKA holoenzyme showing regulatory and catalytic subunits and activation by cAMP. PKA is activated upon binding of cAMP to receptors on the regulatory subunit dimer. This prompts dissociation and release of the catalytic subunits, which are then free to phosphorylate other proteins.

Importance of TORC2 in Chemotaxis

TORC2 (a target of rapamycin complex) plays a central role in the chemotaxis signaling cascade. It is responsible for regulating ACA (Adenylyl Cyclase A) activity, which is key in signal relay to other cells. We are interested in learning more about the RasC-TORC2-PKB/PKBR1 signaling pathway (Figure 1.4). In particular, the research presented in this thesis focuses on the role of PKA (protein kinase A) in controlling TORC2 function and chemotaxis.

Preliminary data suggests that PKA may play a key role in the signaling pathways regulating cell migration in *Dictyostelium* and higher organisms. PKA itself is an enzyme which responds to intracellular levels of cAMP and, in turn, plays a role in the regulation of many well-studied cellular processes including metabolism, memory, and long-term potentiation, as well as several developmental processes unique to *Dictyostelium*.[16]

In higher organisms, PKA is a holoenzyme consisting of two regulatory subunits, each bound to the active site of a catalytic subunit (see Figure 1.5). The enzyme is activated when cAMP binds to the regulatory subunit dimer, prompting release of the catalytic subunits; the catalytic subunits are then active and free to phosphorylate other proteins. In *Dictyostelium*, PKA is a heterodimer composed of only one catalytic and regulatory subunit each.[16]

Both pkaC and pkaR null mutant *Dictyostelium* strains are viable and have been used in various genetic and biochemical experiments in the past.[17–19] Because they lack the catalytic subunit, *pkaC*- cells have no PKA activity. Conversely, *pkaR*- cells (lacking the PKA regulatory subunit) display constitutively active PKA activity.[20] In the experiments presented in this thesis, these cell lines were studied alongside AX3, a wild-type *Dictyostelium* cell line used as a control.[21] AX3 is an axenic strain which means that it is a selected derivative that is able to grow

in a liquid media as a pure culture, free of bacteria and other organisms.[22] These cells grow in liquid HL-5 medium which is a substitute for the bacteria that they would consume in their natural habitat.[23]

Preliminary data

Although it is known that TORC2 functions as a central integrative component of the chemotactic signaling network, it is still not well-understood how it is activated and inhibited. This is critical because cells cannot adapt to changing conditions without the ability of TORC2 to switch between activated and inactivated states. The motivation for this project comes from preliminary data suggesting a possible negative feedback loop between PKA and TORC2.

Preliminary studies have found that, upon stimulation with chemoattractant, cells lacking TORC2 have elevated and extended Rap1 activity levels similar to those observed in PKA null cells (Figure 1.6.A). This suggests that TORC2 may negatively regulate Rap1 during chemotaxis and that this TORC2-dependent inhibition of Rap1 may be mediated by PKA. Furthermore, *pkaC*- cells were also found to have elevated and extended TORC2 and PKB activation (Figure 1.6.B and C). Sca1 was also observed to be highly phosphorylated at PKB sites (Figure 1.6.D), a likely consequence of the elevated PKB activity. PKB phosphorylation of Sca1 inhibits its activity, thus causing reduced membrane localization of the Sca1 complex (Figure 1.6.E) and reduction in RasC activity as a result (Figure 1.6.F). Interestingly, cells with constitutive PKA activity (*pkaR*-) also display elevated and extended TORC2 activity, mirroring the up-regulation of activity seen in *pkaC*- cells (see Figures 1.6.B and 1.7).

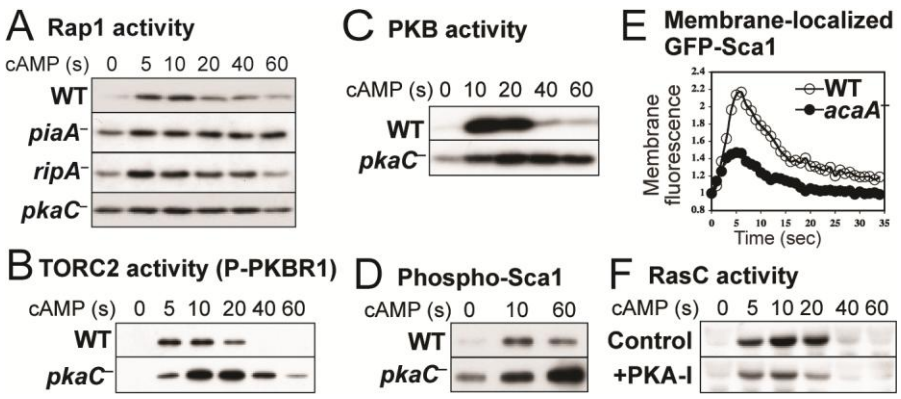

Figure 1.7. PKA-mediated negative feedback regulation of Rap1 and TORC2. **A.** Chemoattractant-induced Rap1 activity is elevated and extended in cells lacking TORC2 or PKA. Cells lacking PKA activity [pkaC null, acaA null, or treated with the PKA inhibitor H89 (PKA-I)] also display elevated TORC2 activity (**B**), PKB activity (**C**), and Sca1 phosphorylation (**D**), but reduced Sca1 membrane localization (**E**) and RasC activity (**F**). (courtesy of Pascale Charest)

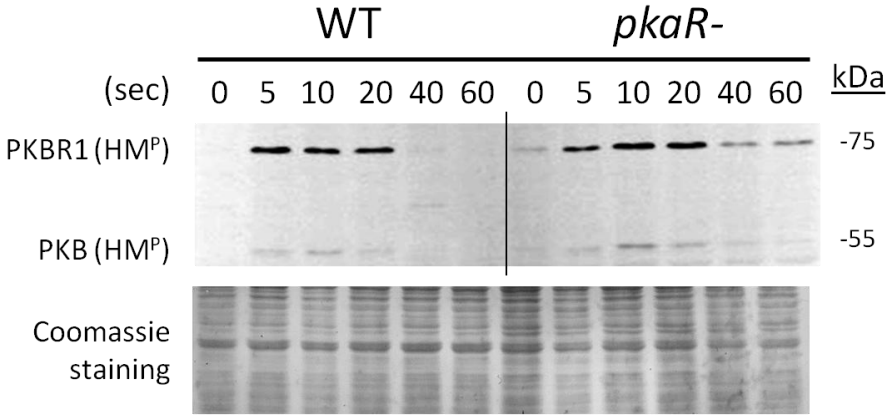

Figure 1.8. PKA regulates TORC2 activity. TORC2 activity is elevated and extended in cells with constitutive PKA activity. This assay detects phosphorylation of PKB/PKBR1 HM (hydrophobic motif) which is mediated by TORC2, thus providing a measure of TORC2 activity.

Taken together, these preliminary results suggest that PKA controls the TORC2 chemotactic signaling network through negative feedback of Rap1. Since Rap1 is a regulator of the cytoskeleton and cell polarity, the PKA-mediated regulation of Rap1 may represent the mechanism by which PKA controls cell polarity during chemotaxis. Figure 1.8 presents a conceptual model of the proposed link between PKA and the TORC2 chemotactic signaling network. The research presented in this thesis aims to characterize the chemotaxis phenotype of cells with misregulation of PKA activity; pinpoint the effects of PKA on F-actin and Myosin II, two cytoskeletal proteins known to play a role in cell polarity and chemotaxis; and, finally, lay the groundwork for future experiments probing the nature of PKA's role in controlling chemotaxis.

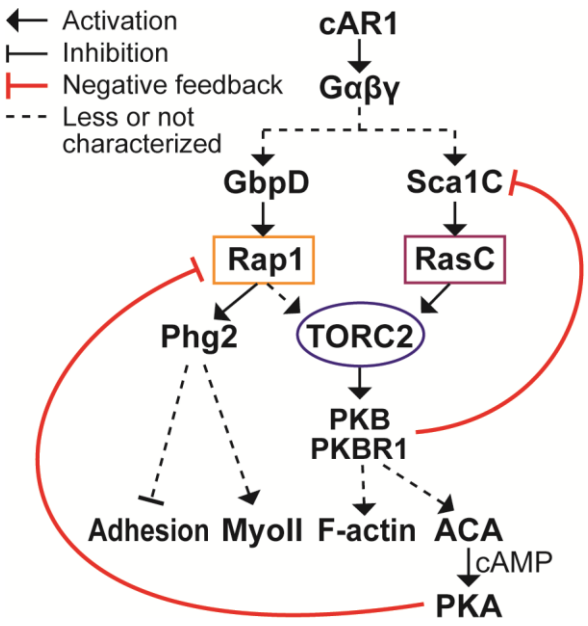

Figure 1.9. A conceptual model of the proposed mechanism for regulation of Rap1 by PKA. This model illustrates the possible inhibition of Rap1 by PKA, leading to lowered TORC2 activity and misregulation of downstream cytoskeletal proteins (including Myosin II and F-actin). (courtesy of Pascale Charest)

Chapter 2. Materials and Methods

2.1 Chemicals and Specialty Equipment

1 kb DNA ladder	NEB
Acetic acid	EMD (VWR)
Agar, granulated	Apex (Genesee)
Agarose	Fisher
Ampicillin	Fisher
Antibiotic/antimycotic	JR Scientific (VWR)
Bio-Rad *DC*™ Protein Assay kit reagents	Bio-Rad
BSA	Amresco (VWR)
cAMP (Adenosine 3',5'-cyclic monophosphate sodium salt monohydrate)	Sigma
Coomassie Brilliant Blue R-250	Amresco (VWR)
DMSO	EMD (Fisher)
dNTP mix	NEB
DTT	Fisher
Ethanol	Stores
Ethidium bromide	Amresco (VWR)
GeneRuler 1 kb DNA ladder	Thermo
Geneticin G-418 Sulfate	Fisher
Glycerol	BDH (VWR)
HL-5 powder (with glucose)	Formedium
Isopropanol	Fisher
KH_2PO_4 (potassium phosphate, monobasic)	BDH (VWR)
Methanol	Stores
Na_2HPO_4 (sodium phosphate, dibasic)	Fisher
NaOAc (sodium acetate)	Amresco (VWR)
PageRuler Plus Prestained Protein Ladder	Thermo
Powdered milk	Albertsons
RNaseA	Invitrogen
SDS (sodium dodecyl sulfate)	Fisher
Sodium chloride	Fisher
Sucrose	Fisher
TEMED	Fisher
Tris(hydroxymethyl)aminomethane hydrochloride (Tris)	Fisher
Yeast extract	Apex (Genesee)

Ismatec IPC pulsing machine	Ismatec (IDEX)
Femtotips®, 0.5 µm inner diam, 1.0 µm outer diam	Eppendorf

2.2 Molecular Biology (Kits, Enzymes, Cells, and Antibodies)

DNA Clean and Concentrator™	Zymo Research (Genesee)
KOD Hot Start DNA Polymerase	Novagen (EMD)
PureLink® Quick Gel Extraction Kit	Invitrogen (Life Technologies)
PureLink® HiPure Plasmid Midiprep Kit	Invitrogen (Life Technologies)
PureLink® Quick Plasmid Miniprep Kit	Invitrogen (Life Technologies)
Zymoclean™ Gel DNA Recovery Kit	Zymo Research (Genesee)

Unless otherwise mentioned, commercial kits were used according to the protocol supplied by the manufacturer.

All enzymes and their respective buffers were purchased from NEB, with the exception of RNase A, which was purchased from Invitrogen:

BamHI-HF
BglII
DpnI
NgoMIV
SpeI
Calf intestinal alkaline phosphatase (CIP)
RNase A
T4 DNA ligase
Taq DNA polymerase (Mg-free)

DH5α bacteria, *pkaR*- cells, and *pkaC*- cells were from common lab stocks (established by Pascale Charest)

Antibodies:

Goat Anti-Mouse IgG DyLight 800	Thermo (Fisher)
Goat Anti-Rabbit IgG DyLight 800	Thermo (Fisher)
Living Colors® Monoclonal GFP Antibody	Clontech
Phospho-p70 S6 Kinase Mouse mAb	Cell Signaling

2.3 Primers and Oligonucleotides

All sequences are in the 5’ to 3’ direction. Self-designed primers were ordered through Sigma-Aldrich, while other primers used for sequencing and PCR were obtained from common lab stocks.

AP1: AAGTGAGATCTAAAAAATGGGTGTTGCTGATTTAATTAAGAAATTCGAATCAATC

- For amplification of Lifeact-GFP (forward)
- BglII-Kozak-Lifeact$_{ATG}$-f

AP2: AAGTGACTAGTTTATTTGTATAGTTCATCCATGCCATGTGTAATCCC

- For amplification of Lifeact-GFP (reverse)
- SpeI-STOPGFP-r

AP3: AAGTGGGATCCGGTGGTTCAGGTATGAATCCAATTCATGATAGAACTTCAG

- For amplification of mhcA (myosin II, forward)
- BamHI-linker-mhcA$_{ATG}$-f

AP4: AAGTGACTAGTTTAAGCTTTGAAACCACCAAAGAAATCG

- For amplification of mhcA (myosin II, reverse)
- SpeI-STOPmhcA-r

AP5: CTCCGTAAACACCTCAGTGAAATC

- For sequencing of Myo in pDM328,
- Nucleotides 6193-6216 (mhcA-f)

AP6: GGTAACAAATGCGATCTCCACG

- For sequencing of Rap1
- Nucleotides 349-370 (RapA-f)

AP7: CCAAGCAAAGCTAAAGAAAAATGTGCTTTATTG

- For site-directed mutagenesis of Rap1 (S181E, forward direction)

AP8: CAATAAAGCACATTTTTCTTTAGCTTTGCTTGG

- For site-directed mutagenesis of Rap1 (S181E, reverse direction)

PC373: CCAAGCAAAGCTAAAGCAAAATGTGCTTTATTG

- For site-directed mutagenesis of Rap1 (S181A, forward direction)

PC374: CAATAAAGCACATTTTGCTTTAGCTTTGCTTGG

- For site-directed mutagenesis of Rap1 (S181A, reverse direction)

2.4 Cell Culture

2.4.1 Growth and Maintenance of Cell Lines

Unless otherwise specified, cells were grown on cell culture dishes in HL-5 medium containing antibiotics mix (pen/strep/fung) and taken directly from plates during log phase growth for experiments.

For selection of transformed cells, G418 was added to prepared HL-5 medium at a final concentration of 20 μg/mL (termed "G20 medium").

Stocks of cell lines were maintained at -80°C in media containing DMSO and thawed as needed.

2.4.2 Transformation of Dicty cells by Electroporation

[Note: Unless otherwise mentioned, all manipulations of cells and DNA involved were performed under sterile conditions in a biological safety cabinet.]Cells were taken directly from plates and counted. The necessary amount was transferred to a centrifuge tube for pelleting (10^7 cells/transformation). Cells were centrifuged for 3 mins at 1200-1500 RPM before removing media in a sterile cell culture hood and replacing it with 40 mL of chilled NaKP buffer (12 mM KH_2PO_4, 12 mM Na_2HPO_4). The cells were centrifuged again, buffer was aspirated, and the tube of pelleted cells was left to incubate on ice for 15 mins. Cells were then resuspended at 10^7 cells/mL in chilled electroporation buffer (10 mM Na/KPO_4, 50 mM sucrose) from which 800 μL were taken and mixed gently with 20 μg of precipitated plasmid DNA (see separate procedure, Section 2.6.5). The mixture was then incubated on ice 1 min, transferred to a sterile chilled electroporation cuvette and pulsed twice (1kV, 3mF, λ-time 0.7-0.9). The transformed cells were then

transferred to a 50 mm dish containing 12 mL HL-5 medium and allowed to adhere and grow overnight. The following day, the HL-5 media was carefully removed and replaced with G20 selection medium.

2.5 Pulsing Dictyostelium cells with cAMP

Pulsing was utilized to starve cells and make them chemotactically competent. Vegetative cells were brought to log phase in shaking culture (2-5x10^6 cells/mL) or on plates (50-75% confluency). After harvesting, the cells were counted in a hemocytometer and an appropriate amount transferred to a 50 mL centrifuge tube. [Note: AX3 and *pkaR*- cells were pulsed at 5x10^6 cells/mL at a total volume of 10 mL/flask, while *pkaC*- cells were normally pulsed at 7x10^6 cells/mL at a total volume of 10 mL/flask.] Cells were then pelleted for 3 mins at 1500 RPM before carefully pouring out media and allowing tubes to drain upside down on a paper towel for a few minutes to remove remaining media. Next, 40 mL of 12mM NaKP buffer was added and the centrifuge tubes were shaken to resuspend the cells, which were then centrifuged for another 3 mins. Buffer was discarded as mentioned above, and cells were resuspended at the appropriate concentration in NaKP buffer.

The cell suspension was then transferred to a 250 mL Erlenmeyer flask and the pulsing apparatus was prepared for cAMP delivery. Cells were pulsed at a final concentration of 30 nM cAMP every 6 mins. For most experiments, this entailed filling the pump lines and attached pipettes with 15 µM cAMP in NaKP buffer and delivering 10 µL/sec for 2 secs, with an “Alt” time of 358 secs. Erlenmeyer flasks were fitted with a rubber stopper, through which was inserted the pipette with its tip in close proximity

with the cell suspension. During pulsing, the flasks were shaken at approximately 240 RPM.

2.6 Molecular Cloning

2.6.1 Amplification and Isolation of Insert DNA (PCR)

Insert DNA was amplified using standard PCR protocol. PCR product DNA was isolated using gel electrophoresis on 1% agarose gels with ethidium bromide for detection of bands. PCR product was taken directly and mixed with loading dye according to the manufacturer's suggested protocol (GeneRuler). The mixture was then loaded onto the gel at 25 μL/lane, along with a DNA ladder (premixed). Electrophoresis was performed at 150V for 20-30 mins until isolated bands were seen and checked against the ladder to confirm that the correct product was obtained. Bands were then excised from the gel and DNA was extracted using a commercial kit (Zymoclean™ Gel DNA Recovery Kit) according to the manufacturer's instructions.

2.6.2 Digestion of Plasmid and Insert DNA

Digestions of cloning vectors and insert DNA were performed using commercially available restriction enzymes and buffers from NEB. Plasmid vectors included pDM304[24] (Figure 2.1)[25]; pDM328[24] (Figure 2.2)[25]; and pEXP4(+)[26,27] (Figure 2.3)[25].

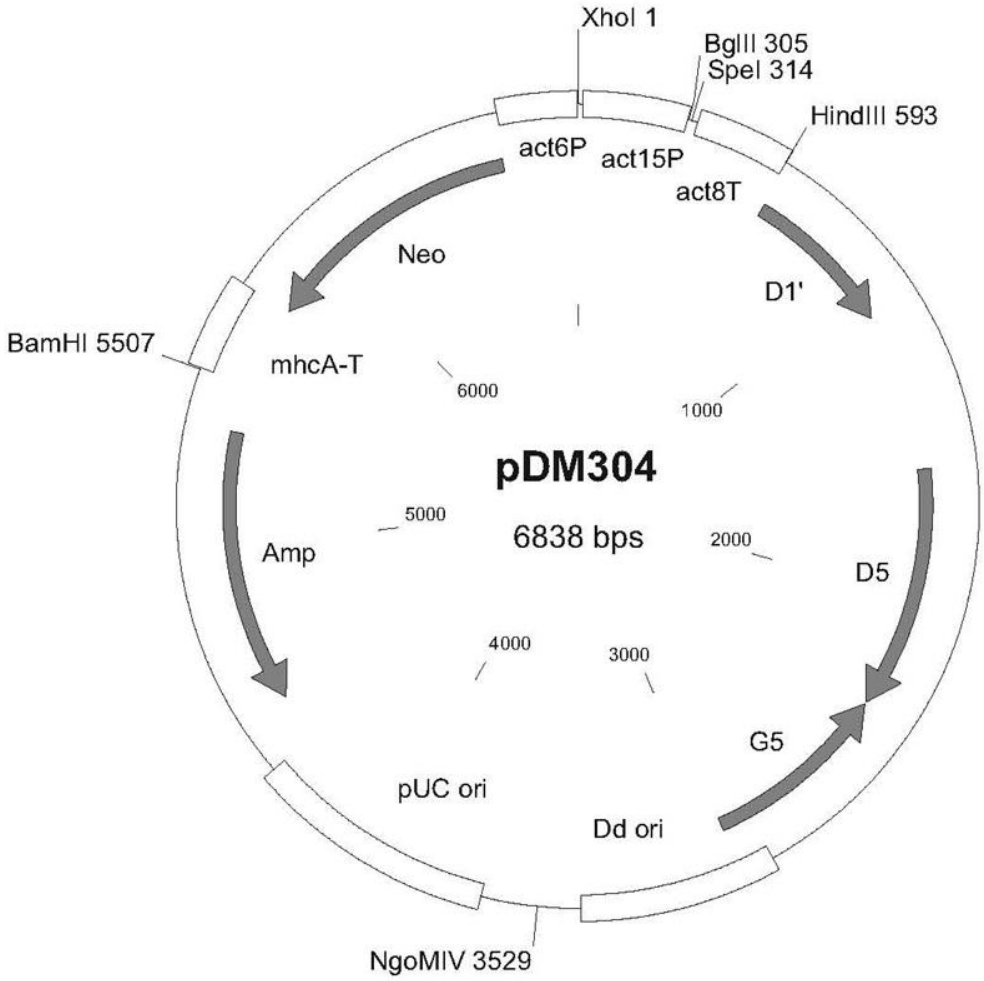

Figure 2.1. Vector map for extrachromosomal expression vector pDM304.[24] (Image from DictyBase; http://dictybase.org/data/plasmid/images/532.jpg).[25]

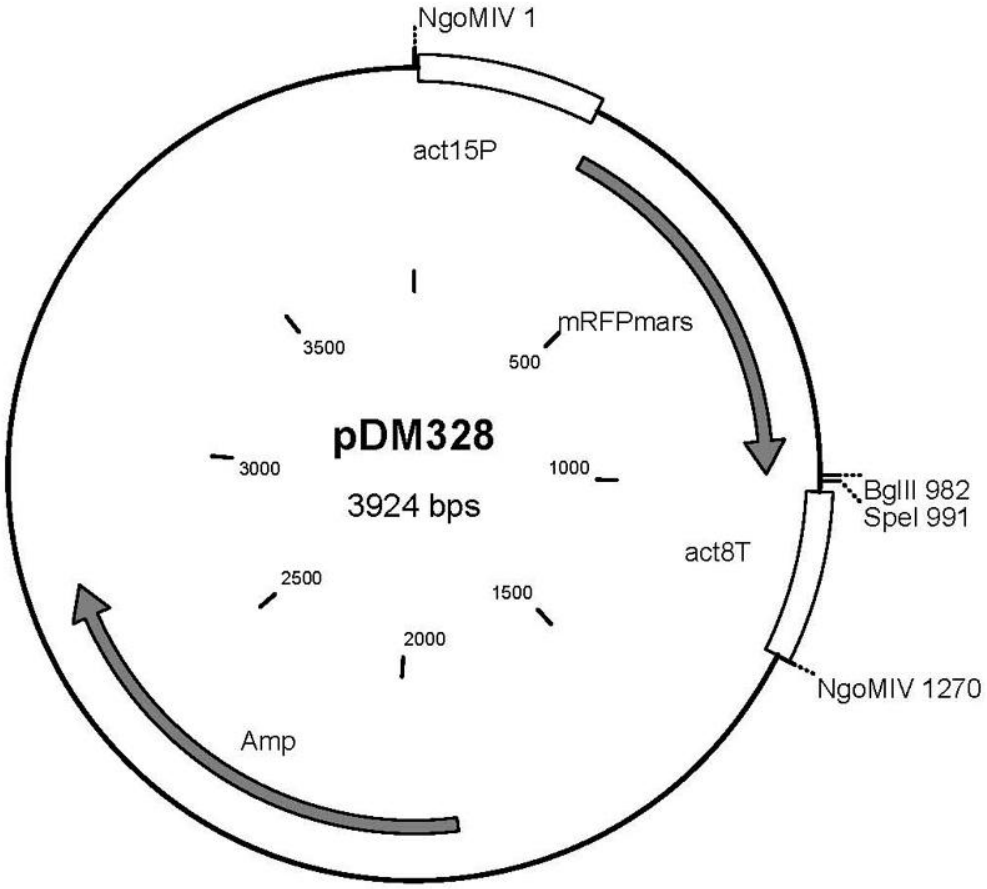

Figure 2.2. Vector map for shuttle vector pDM328, containing N-terminal mRPFmars tag.[24] (Image from DictyBase; http://dictybase.org/data/plasmid/images/553.jpg).[25]

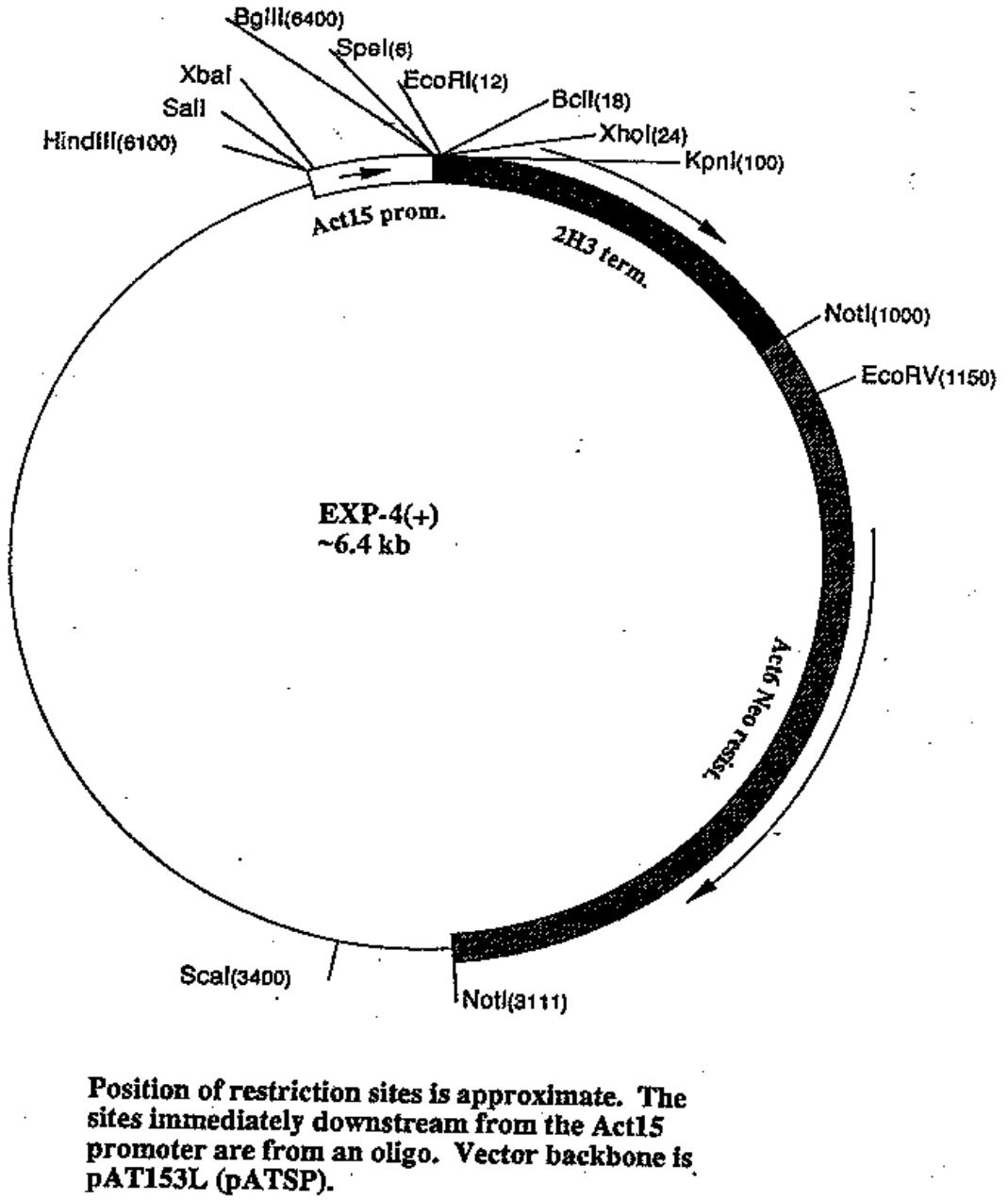

Figure 2.3. Vector map for integrating expression vector pEXP4(+).[26,27] (Image from DictyBase; http://dictybase.org/data/plasmid/images/356.jpg).[25]

2.6.3 Transformation of Competent Bacteria (adapted from Nieves Montaño)

a.) "Long" Transformation—used to transform ligation reactions (cloning)

For each transformation, 100 µL of DH5α bacteria was thawed on ice and 2-20 µL of plasmid DNA was added depending on the total amount of DNA in the ligation/PCR product. After gently flicking the tube to mix, the tube was incubated on ice for 1 hr. A heat shock was performed by incubating the tube at 42°C for exactly 1 min before returning to ice for 2 mins. Next, 400 µL of LB (10 mg/mL bactotryptone, 5 mg/mL yeast extract, 10 mg/mL NaCl) was added to the tube and mixed by flicking the tube. After incubation of the tube at 37°C for 2 hrs (no shaking), different volumes were spread on LB+Amp agar plates (1.5% agar in LB, 0.5 mg/mL Ampicillin) and incubated O/N.

b.) "Short" Transformation—used to amplify supercoil plasmid DNA

For each transformation, 50 µL of bacteria was thawed on ice. Meanwhile, DNA samples received on filter paper were rehydrated in 100 µL of 10 mM Tris buffer (pH 8) and incubated for 15 mins at 37°C and vortexed. After adding 5 µL of DNA (about 500 ng) to the bacteria, the tube was incubated on ice for 30 mins. A heat shock was then performed by incubating the tube at 42°C for exactly 1 min before returning to ice for 2 mins. Next, 400 µL of LB was added to the tube and mixed by flicking the tube. Finally a 50-100 µL aliquot of the transformed bacteria was spread on an LB+Amp agar plate and incubated O/N.

2.6.4 Picking Colonies

After growth O/N on LB+Amp agar plates, transformed bacterial colonies were picked using sterile pipette tips in proximity to a flame to reduce the chance of

contamination. In some cases, PCR screening was utilized screen picked colonies for the plasmid of interest. Pipettes were dropped into sterile glass test tubes containing 2 mL LB + 2 µL Amp. Tubes were then shaken at 37°C and 215 RPM O/N (~16 hrs).

2.6.5 DNA Precipitation (for transformation of Dictyostelium)

DNA was first quantified, and then the appropriate amount was transferred to a sterile tube (usually 20 µg/transformation). To the DNA, 1 volume of 1M NaOAc and 2+ volumes of 100% ethanol were added and the tube was mixed by inverting. The tube was then centrifuged at maximum speed (14,000 RPM) for 10 mins at 4°C. The supernatant was then aspirated, and the pellet was gently washed with 200 µL of 70% ethanol and centrifuged once more, this time for 5 mins. The supernatant was aspirated inside a sterile biological safety cabinet and allowed to dry for 10-15 mins. The dried pellet was then rehydrated with sterile dH_2O to a concentration of 1 µg/µL and dispatched into individual microcentrifuge tubes (1 tube per transform) and stored at 4°C.

2.6.6 Site-Directed Mutagenesis

Site directed mutagenesis for switching of single amino acids was performed using an adaptation of the Stratagene® QuikChange™ Site-Directed Mutagenesis Kit protocol. Mutations were made to residue 181 of the RapA sequence. The template DNA used was mycRap1/pDM358. For each mutation, two oligonucleotide primers were designed (forward and reverse directions) to anneal to the plasmid template and introduce the desired mutation; here, S181A (phosphomutant) and S181E

(phosphomimetic) point mutations were introduced. Sequences for the primers used can be found in Section 2.3.

Four different concentrations of template DNA (5 ng, 15 ng, 25 ng, and 50 ng) were used in the PCR to increase chances of success. Each reaction also contained 125 ng of each primer (PC373 and PC374 for the S181A mutation; AP7 and AP8 for the S181E mutation), 5 µL of 10x reaction buffer, 5 µL of dNTP mix, 3 µL of 25 mM $MgSO_4$, and dH_2O to a final volume of 50 µL. Additionally, a control reaction was prepared that did not contain primers. Finally, 0.5 µL of KOD polymerase was added and the recommended PCR cycling protocol was followed:

1 – 95°C for 30 secs

2 – 95°C for 30 secs

3 – 55°C for 1 min (ramp @ 0.5°C/sec)

4 – 68°C for 10 mins [*recommended 2 mins/kb of plasmid length*]

5 – Go to step 2, 16x [*recommended for single amino acid changes*]

6 – 68°C for 5 mins

7 – Maintain at 15°C until removal

The following day, 2 µL of DpnI (note, twice the recommended amount) was added directly to each PCR product tube and incubated at 37°C for several hours. 2 µL of each digested product was then transformed in 100 µL of DH5α bacteria using the "Long Transform" protocol described in Section 2.6.3.a. Bacteria were then plated (150 µL of each mutation product and 150 µL of un-transformed bacteria to be used as a control) and grown O/N at 37°C. Colonies were picked, grown, and sequenced as per usual.

2.7 Protein Manipulations

2.7.1 Protein Quantification

Protein concentration in cell aliquots was determined prior to gel loading by using the commercially available Bio-Rad *DC*™ Protein Assay kit. A 40 µL aliquot of cells was quantified alongside BSA solutions of known concentration between 0 and 1.5 mg/mL. The absorption of the solutions was measured at 750 nm and a standard curve was prepared to determine protein concentration.

2.7.2 SDS-PAGE Gels

For most Western Blots, SDS-PAGE gels consisted of an 8% separating layer and a 4% stacking layer. Cells used for these experiments were collected in 2X SDS-SB (containing 2% SDS and 100 mM DTT) and stored at 4°C until needed.

Prior to loading on the gel, samples were boiled for 5 mins, spun down, vortexed, spun down again, and cooled to room temperature before loading on gel. Gels were run for 30 mins at 75V to allow migration of samples through the stacking layer, and then run for the remainder of the time at 150V (40+ mins until loading dye had run off the bottom of the gel).

2.7.3 Gel Transfer

Note: Prior to transfer apparatus assembly, all components (fiber sponges, membrane, and filter paper) were pre-soaked in chilled transfer buffer (Tris-glycine). Transfer was carried out in the coldroom for 1 hr at 75 V or 250 mA.

2.7.4 Blocking and Antibody Incubation

Membranes were cut to size prior to blocking and washed in 1X TBS (50 mM Tris, 150 mM NaCl, adjusted to pH 7.4) for 5 mins each. Meanwhile, a 5% powdered milk/TBST (0.1% Tween-20 in TBS) was prepared and thoroughly mixed to eliminate any clumps. Membranes were then blocked for 1 hr at RT. After blocking, membranes were washed 3 times for 5 mins each in TBST. Primary antibody incubation was performed overnight in the coldroom on a rocker, with membranes submerged in antibody solution in homemade Parafilm boats in a covered box.

After primary blotting, membranes were washed 3 times for ten mins each in TBST. Incubation in the secondary antibody was performed for 30 mins at RT in opaque boxes to protect from light. Finally, membranes were washed 3 times for 5 mins each in TBST before imaging.

2.7.5 Imaging

Western blot membranes were imaged using a LI-COR Odyssey with 700 nm and 800 nm channels for detection of either goat anti-mouse or goat anti-rabbit IgG DyLight 800 secondary antibodies. The 700 nm channel was used at very low intensity to assist with identification of bands in the protein ladder.

2.7.6 Coomassie Staining

Membranes were incubated in 0.1% Coomassie Blue in 50% MeOH for 5 mins on a rocker. The stain was discarded and the membrane was destained with several changes of 50% MeOH containing 10% acetic acid, rocking the destain container for

several minutes between solution changes. Finally, the membrane was rinsed for about 5 mins with gentle agitation in H_2O.[28] For long-term storage, membranes were then dried and wrapped in tissue and plastic wrap.

2.8 Microscopy

2.8.1 Imaging System

Confocal fluorescence and DIC images were collected using an Intelligent Imaging Innovations (3i) system built on a Marianas™ (Zeiss Axio Observer) inverted microscope base with a Z-piezo stage (ASI PZ2150FT), Yokogawa CSU-X1 spinning disk, a Photometrics Evolve 512 CCD, and Zeiss Definite Focus. The system is equipped with two lasers for exciting GFP and RFP (488 nm and 561 nm, respectively), and a Photometrics DV2 Dual View splitter to allow imaging with both channels simultaneously. Three objectives were used for different applications: a 20x Zeiss EC Plan-NEOFLUAR (air), a 40x Zeiss EC Plan-NEOFLUAR (oil DIC), and a 63x Zeiss Plan-Apochromat (oil). SlideBook™ versions 5.0 and 5.5 were used for both collecting and analyzing images.

An Eppendorf TransferMan® NK 2 micromanipulator was utilized for cAMP dosing during imaging. The micromanipulator was fixed at a 30-35° angle to the imaging plane to allow for clearance of the tissue culture dishes used for imaging.

2.8.2 Chemotaxis Assays

Cells were pulsed prior to assay as mentioned previously (section 3.2). Dishes for imaging were prepared using plastic tissue culture dishes (35x10mm, Sarstedt) with a 12mm diameter hole punched in the center of each one. Standard vacuum grease was

applied to the perimeter of the hole on the bottom side of the dish and an 18x18-1.5 microscope coverslip (Fisherbrand®) was pressed into place with the grease forming a water-tight seal. Dishes were then filled with ~2500 µL of 12 mM NaKP buffer and 20-50 µL of pulsed cells were added. Cells were allowed to settle and disaggregate for 20-30 mins before imaging. Meanwhile, a femtotip (Eppendorf) was filled with 20 µL of 150 µM cAMP (in NaKP); care was taken to ensure that no bubbles were lodged in the tip. Cells were imaged using a 40x oil-immersion objective. Once the dish of cells was in place, the cAMP-filled femtotip was brought into close proximity with the cells at a 35-degree angle (no more than 10 µm above the cells, and at the opposite edge of the field of view from the cells of interest). Images were then collected every 6 secs for 30 mins (300 frames) in confocal DIC mode with an exposure time of 200 ms.

2.8.3 Random Motility Assays

Cells were grown in shaking culture up to 3-4 x 10^6 cells/mL or taken directly from 30-80% confluent plates. The cells were then washed twice with NaKP buffer and resuspended at 0.1 x 10^6 cells/mL. Imaging dishes were assembled as mentioned above and filled with 3 mL of cell suspension each. Cells were allowed to sit and starve for 1 hr before imaging. Random movement was imaged using a 20x air objective by capturing a frame every 6 secs for 30 mins, and repeated a total of 3 times. Each of the three time-lapse sequences (representing 1, 1.5, and 2 hrs after onset of starvation) was analyzed for cell movement. See Section 2.8.5 for details on cell tracking.

2.8.4 Uniform Stimulation Assays

Cells were pulsed according to standard procedure (see Section 2.5), and cell imaging dishes were prepared as described above. 200 µL of developed cells were added to each dish containing 3 mL of NaKP buffer and allowed to settle and disaggregate for 30 mins before imaging. The microscope was set up to collect time-lapse images every 1 second for 60 seconds with the 63x oil-immersion objective using the appropriate laser (488nm for GFP and 561nm for RPF). Cells were brought into focus and gain, intensification, and laser power were set for each fluorescence channel in use. Image capture was initiated and 100 µL of 150 µM cAMP was rapidly added directly over the field of view immediately after the third image of the series was collected (between 3 and 4 secs).

2.8.5 Cell Tracking

Chemotaxing cells were tracked using the "Manual Particle Tracking" feature within the Mask>Particle Tracking menu in SlideBook 5.5. The feature selected for tracking was Center of Mass. Generally, tracking was not begun until at least the 100^{th} frame (after 10 minutes of cell equilibration with the chemoattractant from the micropipette). A new path was created for each cell within a time-lapse series that did not touch other cells and moved at least one cell-length over the course of the capture. At least 50-100 frames were tracked for each path.

Traces of cell paths were obtained by selecting "Display Paths" under the mask menu. Paths could then be exported within the field of view as a TIF image. Statistics for

tracked cells were exported to Excel for further analysis. “Center of Area” and “Speed” were the features utilized for motion analysis.

2.8.6 Quantification of Fluorescence Intensity

The change in fluorescence intensity over time within the cytoplasm was measured using the *Ratio/Timelapse Data* feature under *Statistics* in SlideBook 5.5. Areas selected for analysis had either a 3 pixel (for smaller cells, such as *pkaC*-) or 5 pixel radius (in the case of AX3 and *pkaR*- cells). Care was taken to choose areas that did not display obstruction or variation due to vesicles or membrane movement during the 60 second collection period. Data was then exported from SlideBook and plotted in Excel as fluorescence intensity versus time. All intensity values in each data set were normalized to the first point in the time-lapse series. Therefore, all values were expressed as an increase/decrease over the basal level on a cell-by-cell basis.

Chapter 3. Results and Discussion

3.1 Characterization of Chemotaxis Phenotype

3.1.1 Results

Before any work could be done to unravel the PKA signaling involved in TORC2 regulation of chemotaxis, it was necessary to characterize the ability of the wild-type (AX3) and PKA mutant cells to migrate toward a cAMP gradient. First, random motility studies were conducted to establish a baseline for cellular movement and compare motility of vegetative cells without the influence of an external chemoattractant signal. Cells were taken from growing culture, washed, and allowed to settle in non-nutritive phosphate buffer. Statistical analysis of random movement was then performed at 1 hr, 1.5 hrs, and 2 hrs after the onset of starvation. Table 3.1 shows several different measures of motility for all three cell lines. Interestingly, speed and distance traveled by AX3 and *pkaC*- cells increased over time, while *pkaR*- cells moved less after longer periods of starvation. However, *pkaR*- cells did move the greatest distance overall, traveling at least twice as far as AX3 and *pkaC*- cells at all time points. Persistence, a measure of path linearity calculated as total linear displacement from beginning to end of the path traveled divided by the total distance traveled, was similarly low in all three cell types; this is expected as movement is random, as opposed to chemotaxis along a chemical gradient.

In understanding the motility defects seen in PKA null cells, it is important to note that there is a clear difference in morphology of each of the PKA mutants versus the AX3 cells. As illustrated in Figure 3.2, AX3 cells exposed to a chemoattractant gradient are elongated and polarized, with a clear front and back. It was also possible to distinguish orientation for *pkaR*-

Strain	Persistence		
	after 60 min starvation	after 90 min starvation	after 120 min starvation
AX3	0.15 ± 0.07	0.15 ± 0.09	0.07 ± 0.06
pkaC-	0.14 ± 0.08	0.15 ± 0.12	0.15 ± 0.11
pkaR-	0.37 ± 0.31	0.14 ± 0.10	0.14 ± 0.11
Strain	Distance (µm)		
	after 60 min starvation	after 90 min starvation	after 120 min starvation
AX3	69 ± 29	76 ± 14	85 ± 21
pkaC-	62 ± 17	66 ± 23	76 ± 24
pkaR-	170 ± 47	158 ± 42	146 ± 43
Strain	Speed (µm/min)		
	after 60 min starvation	after 90 min starvation	after 120 min starvation
AX3	4.0 ± 1.4	5.0 ± 1.0	5.6 ± 1.2
pkaC-	4.0 ± 1.1	4.2 ± 1.4	4.7 ± 1.5
pkaR-	7.4 ± 2.1	6.7 ± 1.8	6.1 ± 1.8

Table 3.1. Statistics for random motility of vegetative cells. Cellular movement was analyzed during three different 30-minute periods after the onset of starvation. Persistence is a measure of path linearity calculated as total linear displacement divided by the total distance traveled. No statistical difference was observed in persistence between cell lines. Distance and speed measurements are illustrated graphically in Figure 3.1. The data above was compiled from 191 individual cell traces.

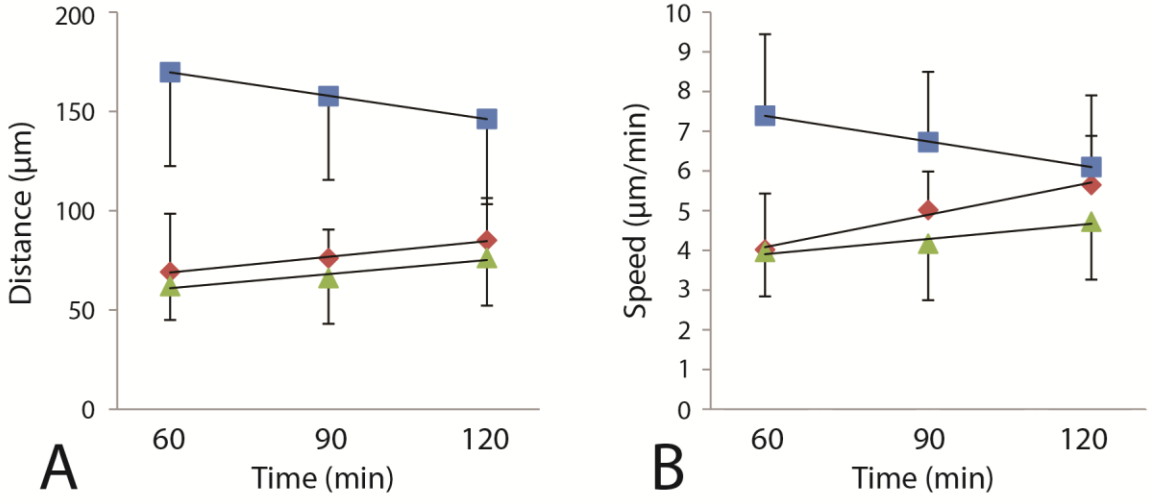

Figure 3.1.A. Non-linear distance moved by vegetative AX3 (◆), *pkaC-* (▲), and *pkaR-* (■) cells as a function of starvation time over the course of a time lapse series. **B.** Speed of vegetative cells at consecutive time points after onset of starvation. Speed is reported as an average of instantaneous speed values obtained by manual tracking of a time lapse series. Each data point represents an average of multiple experiments. Error bars indicate the standard deviation of compiled data for each point.

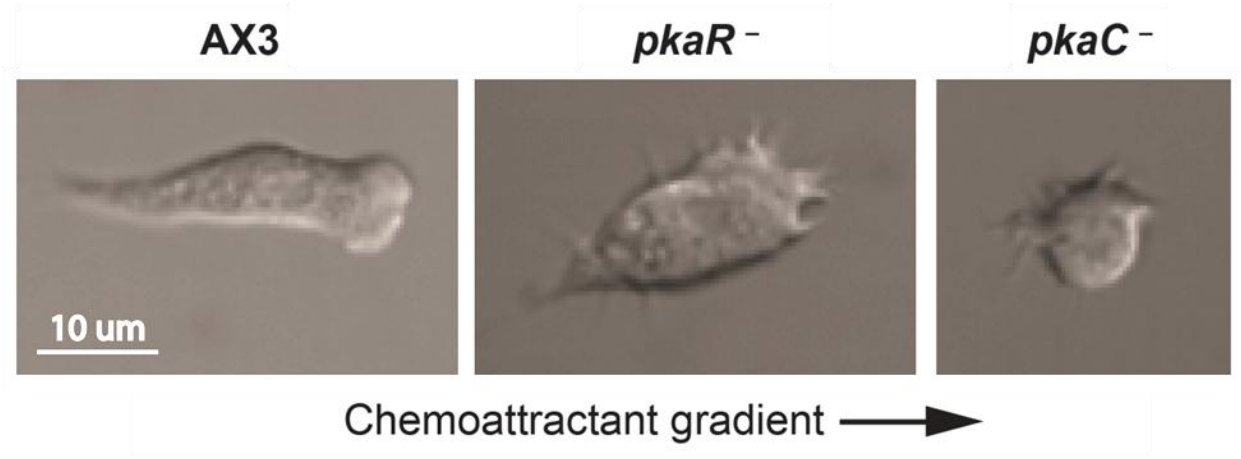

Figure 3.2. Morphology of cell lines studied. Cells pictured were imaged in DIC mode after at least 10 minutes within an established gradient of cAMP and are representative of several experiments.

cells; however, these cells tended to be rounder and thicker than AX3 cells and displayed an increased number of lateral pseudopods. Finally, *pkaC*- cells were much smaller and rounder than both AX3 and *pkaR*- cells and, in most cases, did not polarize in response to the chemoattractant gradient.

Next, it was crucial to characterize (both quantitatively and qualitatively) the ability for each cell type to detect and then respond to a chemical gradient. As described in Section 2.8.2, a micropipette filled with cAMP was introduced to starved cells and time lapse images were collected to record cellular responses. The cells' paths were traced manually using SlideBook's manual tracking feature.

Subsequently, a variety of standard measurements were performed to pinpoint chemotaxis defects in the mutant cells as compared to a wild-type control. Figure 3.3 illustrates representative traces of cell movements and Table 3.2 presents a summary of measurements. In this study, motility speed is defined as an average of the instantaneous speeds measured at each time point, while migration speed is defined as the total linear displacement divided by time. This allows for differentiation between active but undirected movement and directed translocation. Persistence is a measure of path linearity calculated as total linear displacement from beginning to end of the path traveled divided by the total distance traveled. Finally, chemotactic index (CI) was calculated via two different methods. Chemotatic index is an indicator of a cell's ability to move in the direction of the chemoattractant gradient. The general equation used for calculating chemotactic index requires three sets of X,Y coordinates: the starting position of the cell, the ending position of the cell, and the location of the micropipette diffusing cAMP. The equation is as follows:

$$CI = \cos\varphi = \frac{(A^2 + B^2 - C^2)}{2AB}$$

where A represents the chemical gradient vector, B represents the net displacement from beginning to end of the cell's path, C is the distance between the cell's end point and the micropipette, and Φ is the angle indicated on Figure 3.4, below. Each of these variables is calculated using the following equations:

$$A = \sqrt{(x_i - x_m)^2 + (y_i - y_m)^2}$$

$$B = \sqrt{\left(x_i - x_f\right)^2 + \left(y_i - y_f\right)^2}$$

$$C = \sqrt{\left(x_f - x_m\right)^2 + \left(y_f - y_m\right)^2}$$

where the coordinates of the cell starting position are (x_i, y_i); the coordinates of the cell ending position are $\left(x_f, y_f\right)$; and the coordinates for the micropipette are (x_m, y_m).

Taking only into consideration the start point and end point relative to the location of the micropipette diffusing cAMP, it is difficult to conclude that there is a difference between the directionality of AX3 and *pkaR*- cells (see Table 3.2). However, when chemotactic index is calculated at each time point throughout the period of measurement (using the start and end points from one frame to the next relative to the location of the micropipette) and then averaged, it becomes clearer that AX3 cells take a much straighter trajectory than *pkaR*- cells when migrating along a chemical gradient. In both calculations *pkaC*- cells display a very similar

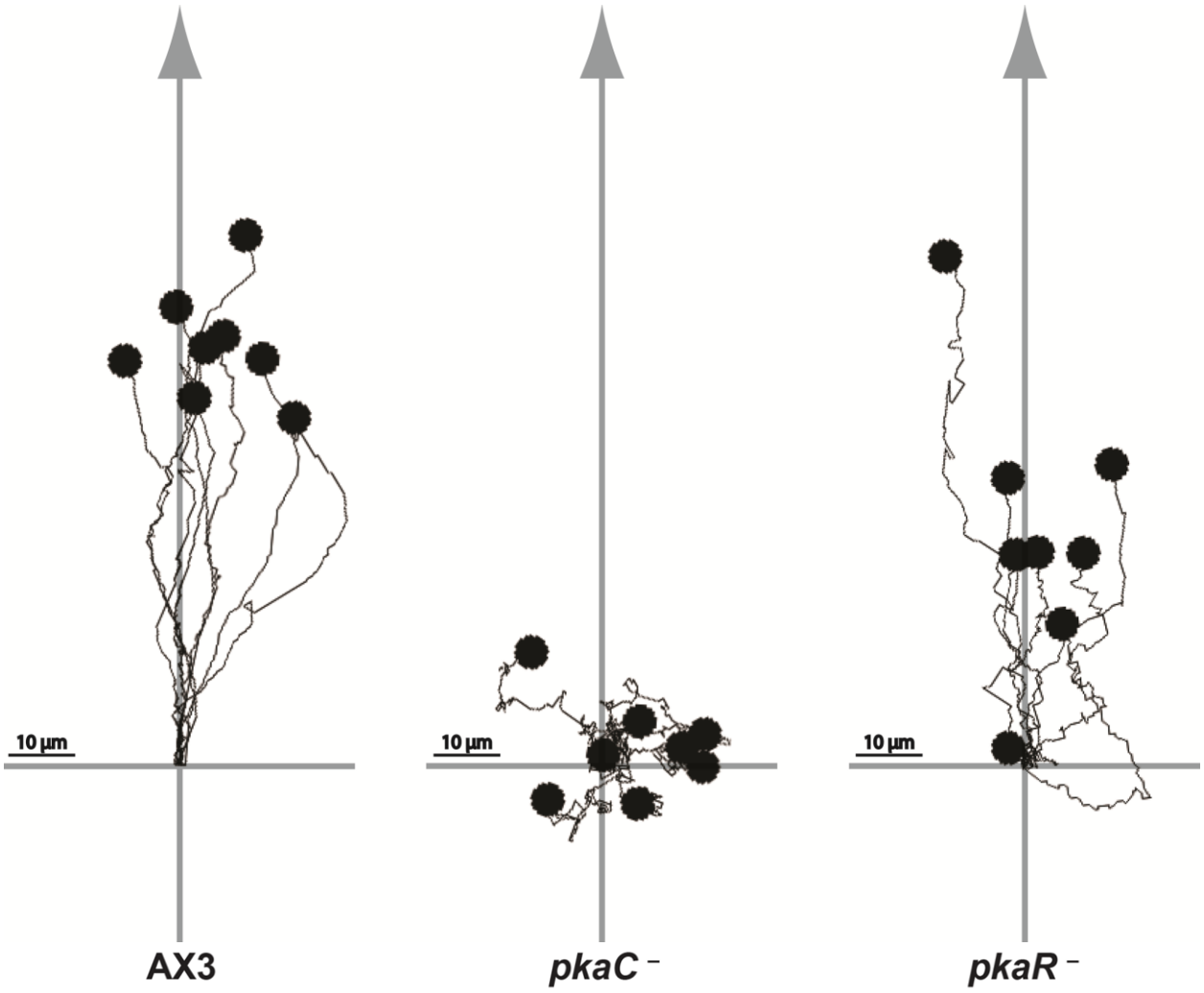

Figure 3.3. Cell traces aligned along a straight path from start position along the cAMP gradient. Black circles indicate the endpoints of traced paths. Traces are aligned with all starting points at the origin of two perpendicular lines and the start and end points positioned relative to a straight line along the cAMP gradient.

Strain	Motility speed (µm/min)	Migration speed (µm/min)	Persistence	Chemotactic index (start to finish)	Chemotactic index (avg over path)
AX3	5.8 ± 0.9	4.7 ± 1.2	0.79 ± 0.09	0.99 ± 0.01	0.76 ± 0.12
pkaC-	4.9 ± 1.4	0.8 ± 0.4	0.16 ± 0.07	0.04 ± 0.59	0.03 ± 0.07
pkaR-	4.7 ± 1.0	2.8 ± 1.5	0.57 ± 0.26	0.91 ± 0.21	0.53 ± 0.27

Table 3.2. Statistics for chemotaxis of starved cells. Motility speed is an average of instantaneous speeds along a path, migration speed is total linear displacement over time, and persistence is a measure of path linearity. Chemotactic index is a fractional indicator of cell movement along the cAMP gradient. Sample sizes: AX3, 10 samples; *pkaC-*, 8 samples; *pkaR-*, 8 samples.

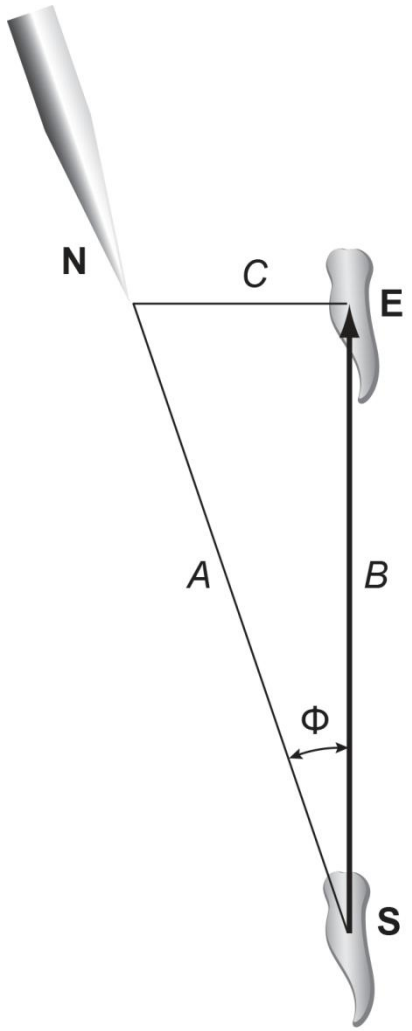

Figure 3.4. Geometric determination of chemotactic index. **S** represents the cell's starting position, **E** represents its ending position, and **N** indicates the location of the micropipette (needle) diffusing cAMP. Φ is the angle between the straight line vector from the cell's start position to the needle (*A*) and the straight line vector from the cell's start to end position (*B*).

chemotactic index, although the second calculation results in much lower error (± 0.59 versus ± 0.07).

In terms of the typical paths taken by these three cell lines, AX3 cells are the most directional while *pkaC*- cells are the least directional (display the most random movements). As expected, all AX3 cells moved in the direction of the chemoattractant gradient and made very few directional changes along the way. Although most *pkaR*- cells eventually traveled toward the micropipette (quantitatively reflected in positive CI values), they tended to change direction extensively along their path, possibly a consequence of their inability to suppress lateral pseudopod formation.[29] As depicted in Figure 3.3, some *pkaR*- cells even initiated movement in the opposite direction of the chemoattractant before correcting their course. Finally, *pkaC*- cells were motile but did not appear to migrate toward the cAMP signal at all. In fact, persistence for these cells did not statistically differ from the persistence values collected during the random motility experiments. From this data we can state that *pkaC*- cells do not perform chemotaxis—rather, they exhibit essentially random movement in a chemoattractant gradient.

3.2.2 Discussion

Two different calculations were performed to obtain a measure of chemotactic index. As seen in Table 3.2 (above), the chemotactic index metric suggests different behavior when calculated using only the start and end points of a cell's path as opposed to taking an average of all movements over the course of the path. The second method more accurately reflects the differences in behavior of AX3 (wild-type) versus *pkaR*- (mutant) cells; however, it is also worth noting that the outcome of this calculation is tightly correlated with the calculation for

persistence. As such, it may not be necessary to report both statistics insofar as they essentially mirror one another and describe the same behavior.

A significant discrepancy is noted when comparing our random motility data (Table 3.1; Figure 3.2) to previously published results.[30–33] Other groups report motility speeds 2-3 times faster than what we observed. When we obtained a new stock of cells from DictyBase (see Figure 3.5), we observed that they were more representative of typical wild-type AX3 cells in terms of their morphology (in particular, their polarization in cAMP gradients); however, their speed was not significantly higher than speeds measured using our original stock.

Many different variables were investigated when attempting to identify the reason for slower motility in our cells. The same frozen stocks of cells used in previous experiments at UCSD were transferred to the University of Arizona with Pascale Charest upon her establishment of the new lab. The same cell culture dishes/coverslips (substrate), media, buffer, chemoattractant, and micropipette for establishment of the chemical gradient were used. Initially, it was hypothesized that a temperature difference may have been responsible for the change in cell motility. It is known that *Dictyostelium* are highly sensitive to changes in temperature outside of a 21-23°C range,[34] so temperature in both the cell culture room and microscope room were carefully monitored. Ambient temperature did not seem to be of concern as it did not deviate significantly from this optimal range, so new cells were ordered from the DictyBase for further testing. These cells were reported to move at speeds of 10-12 μm/min; however, in our experiments they still moved at roughly half that rate.

The tracking software used to measure cell speed was also investigated. Because the observed speed was almost exactly half of the expected speed, it was suggested that perhaps a

calculation error was responsible for the discrepancy. Speed measurements were obtained by manually tracking the center of mass of each cell from one frame to the next throughout a time lapse series. The SlideBook software then exports instantaneous speed at each time point by calculating the displacement of the cell centroid from one time point to the next and then dividing this distance by the elapsed time. This calculation was confirmed by manually measuring the distance moved by a cell in one interval and dividing by time (6 seconds). Finally, the imaging system calibration was checked with the help of Dr. Brooke Beam Massani. The SlideBook software reports a resolution of $0.\overline{66}$ μm/pixel using a 20x objective, which was confirmed to an agreement of 1% by Dr. Beam Massani using a calibration slide (micrometer). As a result, we were able to eliminate calculation/calibration error as a cause for our low reported cell speed.

Finally, we reached out the broad community of researchers working with *Dictyostelium* for suggestions. Surprisingly, multiple researchers suggested that water quality may be a factor (Robert Insall and Pauline Schaap, personal communication). They claim that levels of Ca^{2+} fixation in water used for media and buffers differs greatly depending on the water source used (deionized versus distilled versus Milli-Q), and that this has a considerable effect on cell behavior. Furthermore, it was suggested that vitamins may be diminished during autoclaving, which deprives cells of vital nutrients that they need to thrive. This seems like a viable explanation for the differences we have observed in our experiments since the water source in Biosciences West is, indeed, different than the water used at UCSD (distilled at UA versus Milli-Q at USCD) while all other variables have been held constant. Moving forward, the lab will only use Milli-Q water to prepare all solutions in the hope that this will have some positive effect on

our cell behavior. Furthermore, a DB buffer supplemented with calcium ions will be tested to determine its effect. This buffer is used by the research group of Peter Devreotes, a leader in the field of *Dictyostelium* research, which has consistently reported higher motility/chemotaxis speeds in wild-type cells.[35,36]

Despite deficiencies in cell speed, we are confident that conclusions can be made from the data collected since all experiments were performed under the same conditions and, therefore, we presume that the results for mutant cell lines can be gauged relative to the AX3 control. Figure 3.4 illustrates representative paths taken by wild-type (AX3) and PKA mutant cells in a chemoattractant gradient. Paths of AX3 cells have the straightest trajectory—and thus the highest persistence—of all three cell types studied. Interestingly a significant difference was observed between the two PKA mutants; cells with constitutively active PKA (*pkaR*-) are less impaired in their ability to migrate than are cells with PKA activity completely absent (*pkaC*-). The observation that *pkaC*- cells have the most severely affected phenotype, i.e., they are not able to polarize or migrate in response to a chemoattractant gradient, suggests that PKA activity is required to participate in some sort of feedback loop connected to downstream effectors of cell motility. On the other hand, cells with constitutively active PKA (*pkaR*-) are able to sense the gradient and produce pseudopods; however, the constitutive PKA activity may very well explain the surplus pseudopods and frequent directional changes in these cells. This observation corroborates other evidence suggesting that uninhibited PKA activity also has a deleterious effect on cell motility,[29,37] supporting the theory that this kinase participates in a feedback loop integral to regulation of chemotaxis.

Finally, it is recommended that the random motility data be re-collected. The AX3 measurements presented in Table 3.1 and Figure 3.2 are more than likely inaccurate as they were obtained using an old stock of cells that failed to properly polarize in a chemoattractant gradient (see Figure 3.5, below, depicting morphological differences between old [left] and new [right] wild-type cells). Additionally, a larger data set comprised of at least 40 to 50 cells from each cell line should be collected; it is expected that this will help to minimize the large error observed in Figure 3.2, presumably due to the small sample size (fewer than 30 cells for each data point).

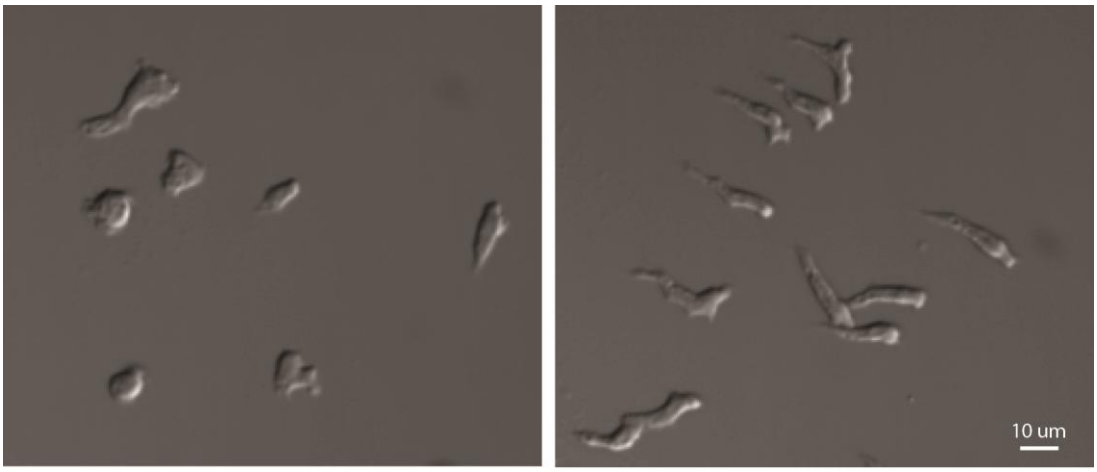

Figure 3.5. Comparison of two different stocks of AX3 cells used in experiments. Images were collected after 30 minutes of exposure to a cAMP gradient. Note that the old stock of cells (left) fail to polarize whereas cells in the new stock obtained from DictyBase (right) elongate and perform chemotaxis more efficiently.

3.2 F-Actin Dynamics

3.2.1 Results

Since significant differences were noted in PKA mutants in terms of their ability to polarize and perform chemotaxis, it was important to examine the crucial cytoskeletal components that enable cell motility. As mentioned previously, both actin and myosin are required to work cooperatively to produce cellular movement. In wild-type cells it has been established that myosin must localize at the back/rear of the cell to provide contractile forces and that filamentous actin (F-actin) must assemble at the front of the cell to produce protrusions and move the cell forward.

An F-actin reporter, Lifeact,[38] was tagged with GFP and used to monitor spatial and temporal localization of actin in AX3 cells and PKA mutant cells. This particular reporter was chosen because it has been shown to be the best F-actin probe currently available.[39] Whereas other actin probes utilize actin-binding domains (ABDs) or fluorescent proteins fused directly to actin, Lifeact binds non-competitively and does not interfere with actin dynamics. It is a 17-amino-acid (non-bulky) peptide derived from Abp140, an actin-binding protein found in *Saccharomyces cerevisiae*, that has been shown to bind to all subsets of F-actin without compromising the integrity and dynamics of the cytoskeleton.[38,39]

Cells transformed with Lifeact-GFP were subjected to two different stimulation experiments to induce localization of actin. The first experiment consisted of uniformly stimulating developed cells and observing their response (see Section 2.8.4 for experimental protocol). The purpose of this experiment is to determine the F-actin polymerization dynamics in response to the chemoattractant. In a resting wild-type cell, signaling molecules and cytoskeletal

components, including actin, are delocalized and randomly distributed in the cytoplasm. When a chemoattractant signal is detected, these components rearrange to create a defined front and back with F-actin expected to polymerize at the leading edge to enable forward movement. By acutely stimulating the cells with cAMP it is possible to observe reorganization of certain proteins to the membrane in response to the chemoattractant. This experiment is valuable because it produces quantifiable data regarding the temporal regulation of F-actin polymerization. For each cell type, multiple experiments were conducted over several days to ensure reproducibility. Cells were uniformly stimulated and then observed for 60 seconds.

As shown in Figure 4.1.A, localization of F-actin (as reported by Lifeact-GFP) in AX3 cells is apparent at the cell membrane with intensity peaking at around 7 seconds post-stimulation. F-actin then begins to delocalize and return to the cytoplasm, returning to basal levels at around 25 seconds after the stimulus. Figure 4.1.B shows quantitative data representing these transitions. To produce this graph, discrete areas within the cytoplasm of starved cells were monitored over the 60-second course of the experiment to record changes in fluorescence over time. These values were normalized to fluorescence intensity at the first time point in each series, representing the basal level. These values were then inverted to produce a graph indicating fluorescence intensity at the cell membrane over time. For each cell line, dozens of discrete areas were independently analyzed and normalized before averaging to produce the trendlines graphed in Figure 4.1.B. Standard deviation among the sample set is represented by error bars.

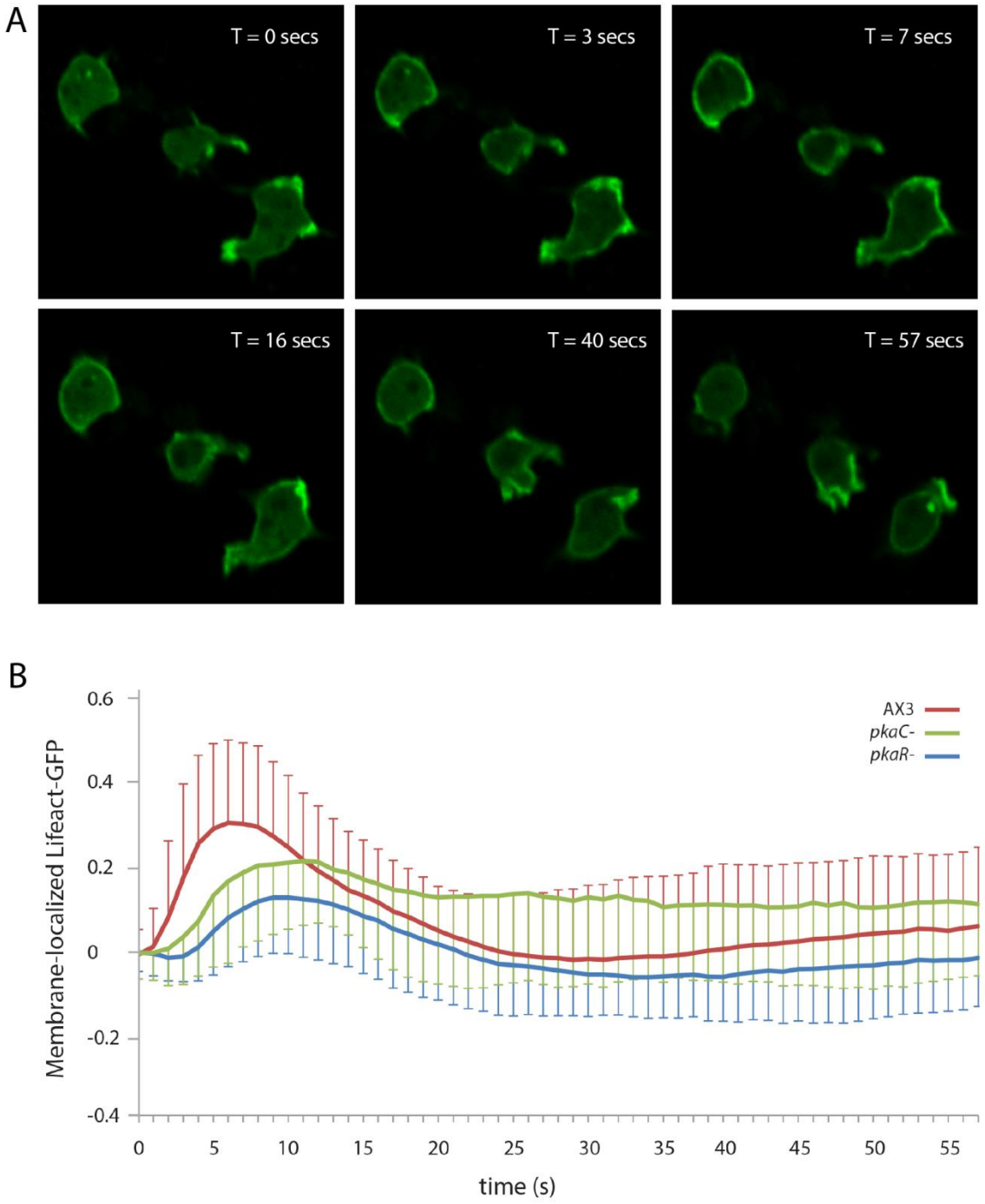

Figure 3.6.A. Response of AX3 cells containing an F-actin reporter to uniform cAMP stimulation. Cells were monitored via confocal fluorescence microscopy over a period of 60 seconds to record their response. F-actin polymerization at the plasma membrane is apparent within 3 seconds after uniform stimulation. **B.** Quantification of membrane-localized Lifeact-GFP (actin reporter) as a function of time. All data was normalized to the basal level of fluorescence at T=0, reflecting an increase and subsequent decrease in membrane-localized Lifeact-GFP after stimulation. Sample sizes: AX3, 70 samples; *pkaC-*, 47 samples; *pkaR-*, 87 samples.

AX3 cells (70 samples) displayed the highest peak at 6 to 7 seconds post-stimulation with cAMP. Furthermore, these cells also displayed a slightly faster response to the stimulus than the mutants, showing an increase from the basal level as early as 1 second after cAMP was introduced. Both *pkaC*- cells (47 samples) and *pkaR*- cells (87 samples) also responded to chemoattractant stimulation, but to a lesser degree. The amplitude of increase over basal level was not only lower than that of the wild-type cells, but also took up to 2 additional seconds to begin increasing. Furthermore, it is interesting to note that the *pkaC*- cells do not return to their basal level of membrane fluorescence within the measured 60-second time period, although levels do decrease slowly. AX3 cells return to their basal levels by 30 seconds followed by a gradual relocalization of actin to the membrane—presumably as the cells begin to resume their normal movement.

The second experiment placed the cells in a chemical gradient of cAMP to observe localization (or delocalization) of F-actin within a cell as it is moving. Cells were allowed to translocate in the cAMP gradient as time lapse images were captured. Figure 4.2 shows actin localization in representative AX3, *pkaC*-, and *pkaR*- cells. There is a clearly observed enrichment of F-actin at the leading edge of polarized AX3 cells, which is to be expected. Interestingly, both PKA mutants display an accumulation of actin at their membrane protrusions despite their chemotactic deficiencies. However, *pkaC*- cells tended to polymerize F-actin all around the perimeter and not necessarily in the direction of the chemoattractant, whereas *pkaR*- cells showed the greatest enrichment of F-actin in their lateral pseudopods.

3.2.2 Discussion

By comparing behavior of wild-type cells with both PKA mutants, we aimed to quantitatively and qualitatively determine discrepancies in spatiotemporal regulation of F-actin and, thus, establish whether or not misregulation of this cytoskeletal component may be responsible for the observed chemotactic deficiencies in cells with absent and constitutive PKA activity. From this we can conclude that, although both mutants are capable of polymerizing F-actin and creating membrane protrusions, the mechanism for this activity is both spatially and temporally misregulated. Although localization is observed, it is not always colocalized with a leading edge as we see in wild-type cells. This inability of PKA null cells to restrict F-actin polymerization to one edge is consistent with the lack of polarization seen in these cell lines; these observations suggest misregulation of the upstream sensing mechanisms responsible for determining the orientation of the gradient and directing the cytoskeletal response accordingly. The next step will be to look at biochemical indicators of protein activity to expose the interactions of upstream signaling pathway interactions that may be responsible for this misregulation.

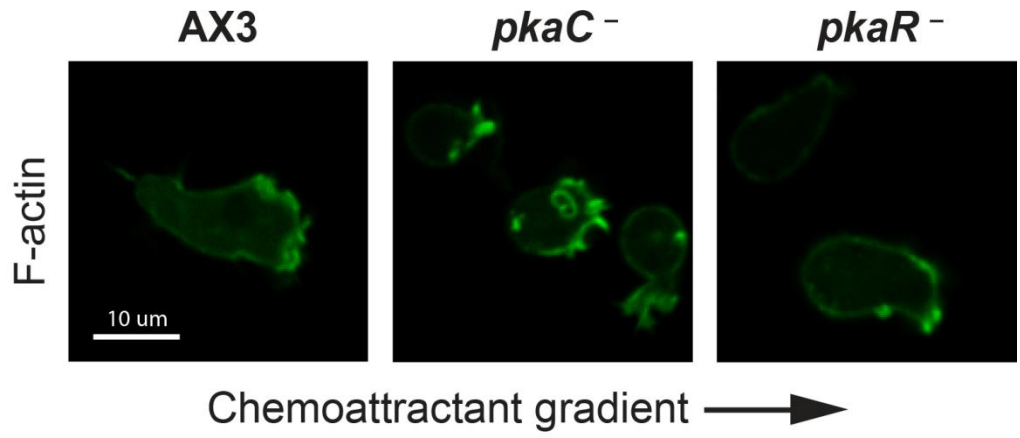

Figure 3.7. F-actin (Lifeact-GFP) localization in chemotaxing cells. The fluorescent reporter indicates enrichment of F-actin at the leading edge of AX3 cells moving in the direction of a cAMP gradient. Both *pkaC*- and *pkaR*- cells display localized F-actin at membrane protrusions when exposed to the same chemoattractant gradient despite their reduced ability to polarize and migrate efficiently; however, this polymerization of F-actin is not confined to the front—especially for *pkaC*- cells—toward the highest concentration of chemoattractant.

3.3 Myosin II Dynamics

3.3.1 Results

After probing actin dynamics in PKA mutant cells, an equally-important objective was to study the spatiotemporal dynamics of assembled Myosin II in these cells. Myosin is a protein long known to be responsible for muscle cell contraction but has also been shown to play a key role in development and motility of non-muscle cells, including *Dictyostelium*.[8,40,41] As mentioned previously, assembled Myosin II is enriched at the sides and posterior cortex of migrating cells to enable contraction and, thus, forward movement of the cell's rear. To track localization of Myosin II, exogenously-expressed GFP-fused myosin II heavy chain was used (GFP-Myosin).[42]

The same experiments conducted with Lifeact-GFP were repeated to visualize Myosin II dynamics in vivo. Briefly, the first series of experiments involved uniformly stimulating starved cells with an external source of cAMP to gauge their response. Figure 5.1 summarizes the results of these experiments. Prior to stimulation, resting cells display a low level of GFP-Myosin localization at the cortex. When stimulated with the chemoattractant, AX3 cells displayed a decrease in membrane-localized GFP-Myosin, indicating translocation of this protein to the cytoplasm (Figure 5.1.A). The removal of GFP-Myosin from the cell membrane was complete by 10-15 seconds post-stimulation. GFP-Myosin then gradually returned to the cell cortex, with a peak increase over basal levels occurring at 30-35 seconds after stimulation. Finally, cortex-localized GFP-Myosin gradually returned to basal levels by around 60 seconds.

In *pkaR-* cells, GFP-Myosin was originally delocalized from the cortex upon chemoattractant stimulation; however, it is interesting to note that, following this initial

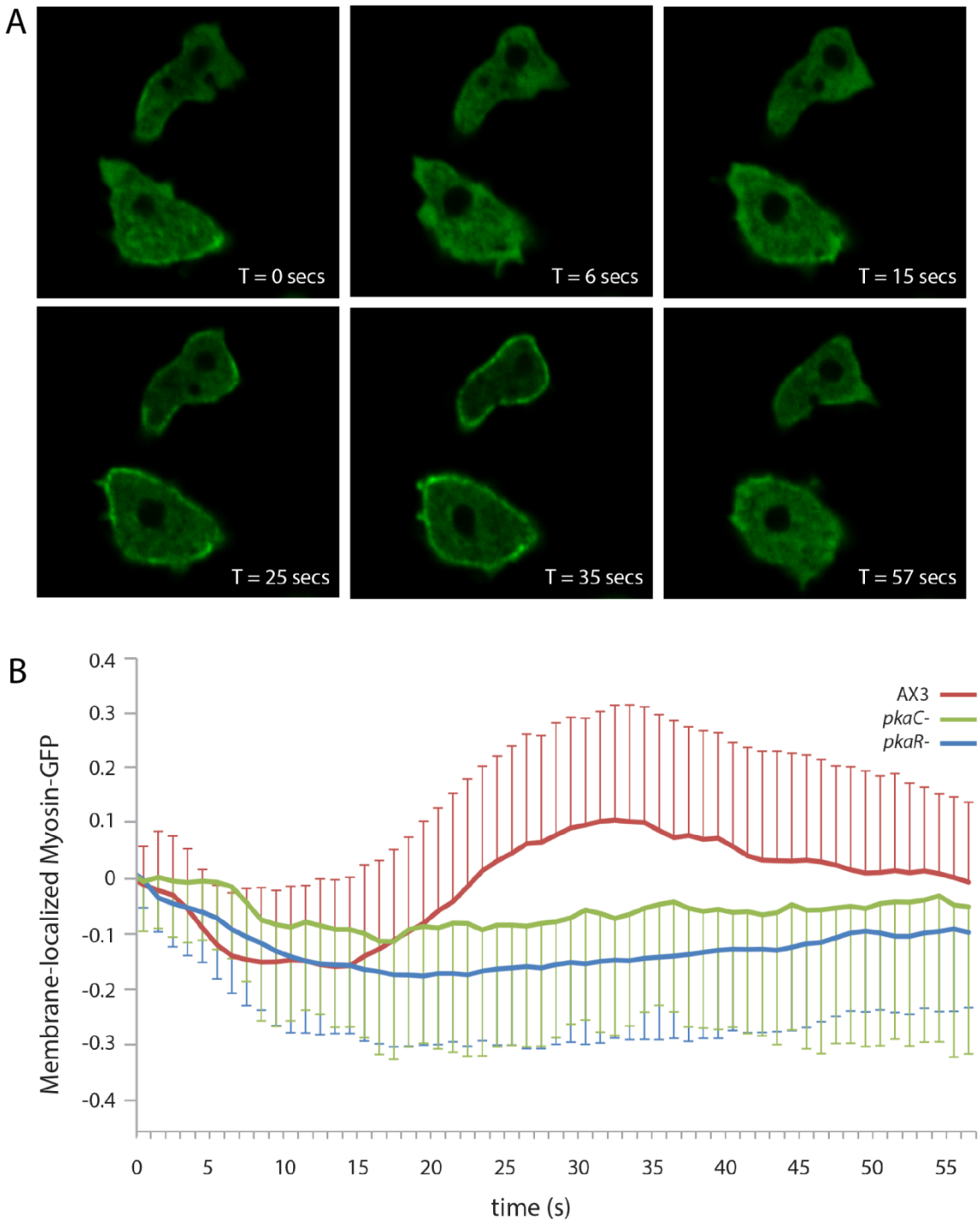

Figure 3.8.A. Response of AX3 cells containing GFP-Myosin to uniform cAMP stimulation. Initially, a low level of cortex-localized GFP-Myosin can be observed. Upon stimulation, GFP-Myosin is delocalized from the cell cortex and moves to the cytosol before it translocates back to the cortex, with a peak around 30 seconds, and goes back to basal levels by 60 seconds after stimulation. **B.** Quantification of membrane-localized GFP-Myosin as a function of time. Sample sizes: AX3, 61 samples; *pkaC-*, 28 samples; *pkaR-*, 54 samples.

delocalization, GFP-Myosin did not become enriched at the cortex as seen in wild-type cells (Figure 5.1.B). Instead, cortex-localized GFP-Myosin only slowly returned to basal levels. In *pkaC*- cells, a clear trend was not observed. There may be a slight decrease in membrane localization upon stimulation, but it is unclear. This can possibly be attributed to either a small sample size or to an actual lack of myosin regulation in these cells.

Enrichment of assembled Myosin II was confirmed at the back and sides of chemotaxing AX3 cells (Figure 5.2), as previously reported.[42] GFP-Myosin was also transiently observed in retracting protrusions in all cell types (not shown). In *pkaC*- cells, GFP-Myosin was evident at the membrane, but to a lesser extent than in AX3 cells. Because these cells tend to move randomly and change direction frequently, extended periods of localization were not observed. Finally, as seen in Figure 5.2, GFP-Myosin localization in *pkaR*- cells was largely similar to that of wild-type cells. As it is characteristic of *pkaR*- cells to display an increased number of lateral pseudopods, GFP-Myosin was also repeatedly observed in these protrusions as they were retracted back into the cell body.

3.3.2 Discussion

Myosin II response to stimulation occurs out of phase with the F-actin response—both cytoskeletal components should not be active at the same time. This can explained as an alternation between *protrusion* of the leading edge, which occurs via F-actin polymerization, and *traction* of the back end, which is a result of myosin-dependent contraction.[43] This is clearly observed in the wild-type when comparing the AX3 traces in Figures 5.1.B and 4.1.B. To the contrary, both *pkaC*- and *pkaR*- cells produce a relatively flat trace, indicating a subdued response to the chemoattractant.

When addressing the observed differences between wild-type and mutant cells in this study, perhaps the most obvious is the very slow response *pkaR*- cells. Cytoskeletal reorganization is less efficient and of a lesser magnitude than in wild-type cells. It is also important to note the difficulty in collecting data from *pkaC*- cells due to their small size and a prevalence of free-floating vesicles within the cytoplasm. When analyzing the time-lapse series for this cell line, the vast majority of cells could not be used for fluorescence intensity analysis due to either vesicular obstructions moving throughout the cytoplasm or lack of sufficient cytoplasmic area for analysis. Although more data needs to be collected for these cells, the preliminary results in Figure 5.1.B suggest that *pkaC*- cells have a misregulation of myosin.

Myosin was excluded from protrusions in all cell lines, which suggests that signals upstream are causing polarization, not necessarily actin and myosin. Both cells lacking PKA activity and cells with high PKA activity seem to be unable to properly regulate the assembly and disassembly of myosin II. This cytoskeletal defect, along with failure to localize F-actin, very likely underlies the inability of *pkaC*- cells to polarize and migrate. Because myosin II assembly—not only at the rear of the cell but also at the sides—is crucial for polarization, this could explain both the inherent roundness of *pkaC*- cells and the overabundance of lateral pseudopods forming in *pkaR*- cells (myosin II assembly at the lateral sides of the cell is essential to suppress these).

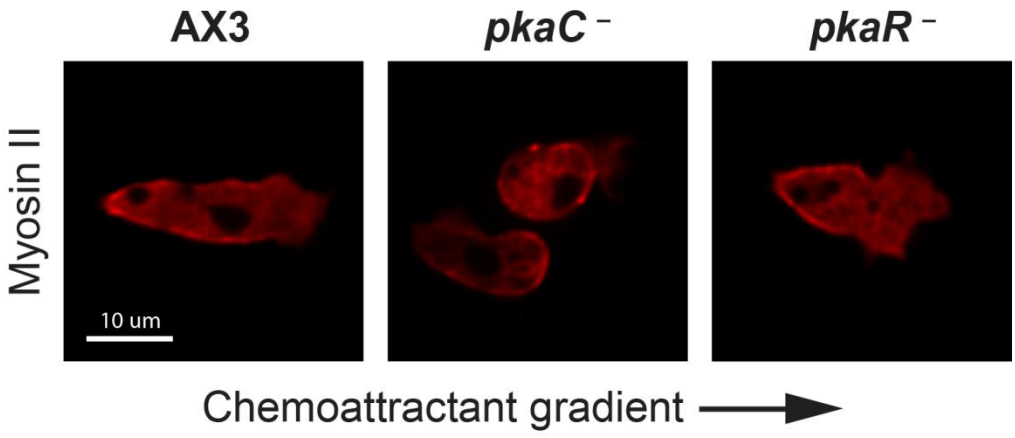

Figure 3.9. GFP-Myosin in chemotaxing cells. The fluorescent reporter indicates assembly of Myosin II at the sides and posterior of AX3 cells chemotaxing in a cAMP gradient. Both *pkaC*- and *pkaR*- cells display localized GFP-Myosin when exposed to the same chemoattractant gradient despite their reduced ability to polarize and migrate efficiently. Note that localization of GFP-Myosin in the *pkaC*- cells pictured is oriented on the edge closest to the source of the chemoattractant. This is due to the cells migrating away from (instead of toward) the gradient—further highlighting their chemotactic deficiencies. GFP-Myosin is represented as pseudocolor red.

3.4 Actin/Myosin Dual Reporter Construct

3.4.1 Results

Initially, we planned to produce a DNA construct containing reporters for both F-actin and Myosin II to enable visualization of both cytoskeletal components simultaneously in stimulated cells. Lifeact-GFP was cloned into pDM304, an extrachromosomal expression vector.[24] Next, myosin II heavy chain A (*mhcA*; Myosin) was amplified via PCR using AP3 and AP4, primers designed for this purpose. The sequence for the forward primer is shown in Figure 6. The amplified Myosin insert was then cloned into the BglII/SpeI site of pDM328, a shuttle vector containing the sequence for mRFPmars.[24] The resulting plasmid was then digested using NgoMIV such that the segment containing RFP-Myosin could be isolated and inserted into the NgoMIV-digested pDM304 vector already containing Lifeact-GFP (see Figure 6.2). The resultant plasmid was then electroporated into cells which were selected based on their G418 resistance and imaged.

In chemotaxing wild-type cells, it was discovered that Lifeact-GFP was, indeed, localized to the leading edge as predicted. Unfortunately, RFP was only observed in the cytoplasm (Figure 6.3). A Western blot was then run to ascertain whether the RFP was fused to Myosin (not shown). A single band was observed at approximately 55 kDa upon detection with a GFP antibody. Because GFP variants weigh roughly 27 kDa, we presume that this band represents an RFP dimer. This supports our hypothesis that RFP had been cleaved from Myosin, explaining the presence of only cytosolic RPF in imaged cells.

3.4.2 Discussion

The linker sequence introduced via the AP3 primer is hypothesized to be responsible for cleavage of RFP from myosin within cells. Commonly, polypeptide linkers of 2 to 10 amino acids in length are chosen when fusing fluorescent proteins to a protein of interest. In this case, a Gly Gly Ser Gly linker was utilized because of the flexibility these amino acids confer. Because another construct made in the Charest lab using the same linker sequence also led to degradation of the fusion protein (data not shown), it is possible that this sequence may be a target for a *Dictyostelium* protease which degrades the fusion protein.

Future studies on other cell lines will very likely also require actin/myosin reporters, so attempts at making this dual-reporter construct are ongoing. Other members of the lab, Dr. Tariq Islam and Branden Stepanski, have modified the cloning strategy to eliminate the linker between RFP and Myosin, and are in the process of screening, sequencing, and testing the new construct. There is great potential in this dual-reporter design as it will eliminate the additional steps required to electroporate cells with F-actin and Myosin II reporter constructs separately, as was done in this study. Furthermore, the confocal fluorescence imaging system used to collect the images presented in this thesis is equipped with a Photometrics Dual View (DV2) splitter which permits simultaneous imaging with both the 488 nm and 561 nm channels, potentially expediting the collection of data and producing images with greater visual impact.

AP3 (5nt-BamHI-(linker)-mhcA$_{ATG}$-f)

AAGTG GGATCC GGTGGTTCAGGT ATGAATCCAATTCATGATAGAACTTCAG

Figure 3.10. Sequence for forward oligonucleotide used to amplify *mhcA* (Myosin). The sequence begins with a 5-nucleotide sequence to initiate annealing and anchor the primer. This is followed by the 6-nucleotide sequence for BamHI to introduce a restriction site for cloning. Next, the sequence for a linker (GGSG) is inserted to permit flexibility upon fusion of Myosin and mRFP. Finally, the first 28 nucleotides in the *mhcA* sequence are included to initiate amplification of the gene.

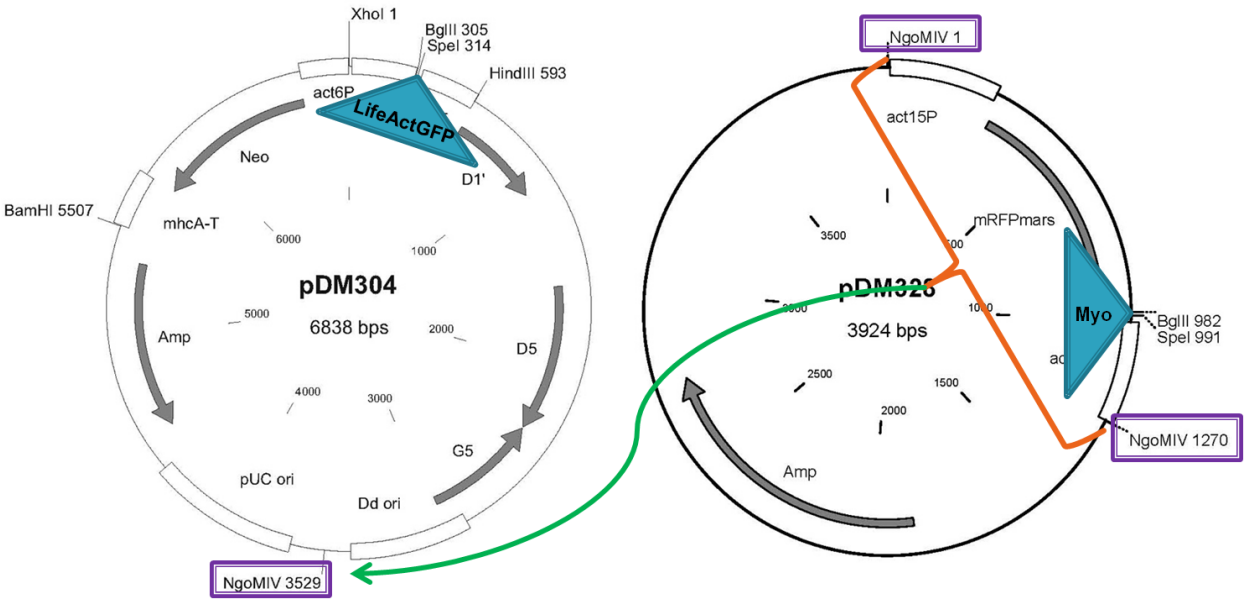

Figure 3.11. Cloning strategy for LifeactGFP/RFP-Myosin in pDM304. Lifeact-GFP was cloned into the BglII/SpeI double-digest restriction site of vector pDM304. Myosin was then amplified via PCR and cloned into the BglII/SpeI double-digest restriction site of shuttle vector pDM328 containing the sequence for mRFPmars. The resulting plasmid was then digested with NgoMIV to remove the cassette containing mRFPmars-Myosin; this was then cloned into the NgoMIV restriction site in the Lifeact-GFP/pDM304 construct.

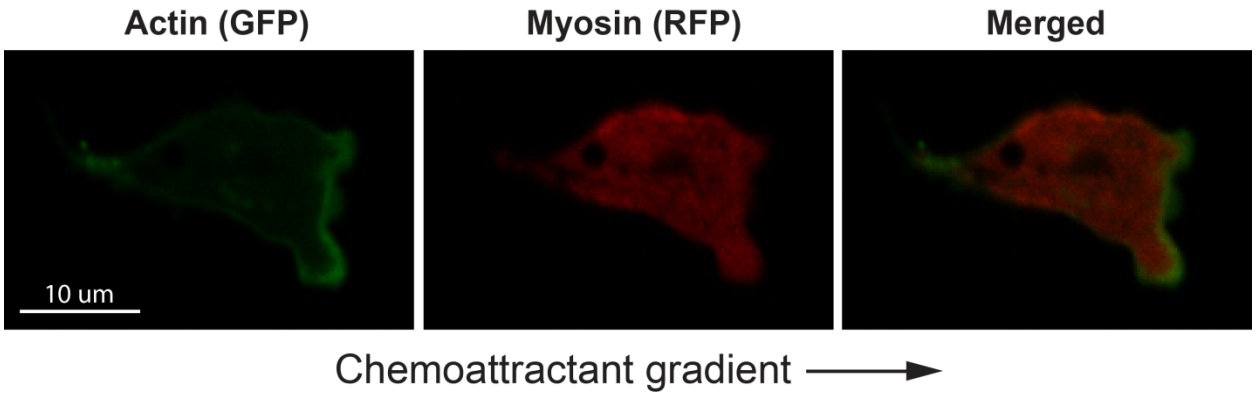

Figure 3.12. Investigating the spatiotemporal dynamics of F-actin and RFP-Myosin in wild-type cells using the tandem-expression construct Lifeact-GFP/RPF-Myosin/pDM304. F-actin is enriched at the leading edge as anticipated, whereas Myosin II is not enriched at the sides and rear of the chemotaxing cell.

3.5 RBD-GFP Assays

3.5.1 Introduction

In the attempt to elucidate the role of PKA in chemotactic signaling, one possible mechanism to investigate is PKA regulation of TORC2 through Ras/Rap proteins. Ras proteins comprise a sub-family of proteins under the category of small GTPases. Ras signaling plays a key role in cellular signal propagation by activating other proteins. In particular, RasC is known to be activated upstream of TORC2 upon stimulation with cAMP.[44] Because we have evidence that RasC is regulated either directly or indirectly by PKA (see Figure 1.6.F in Introduction), preliminary data was collected to monitor spatiotemporal regulation of this protein in PKA mutant cells. This was achieved by using a Ras activity reporter consisting of the Ras binding domain of the human protein Raf-1 fused to GFP (RBD-GFP).

RBD-GFP has been shown to bind to GTP-bound (active) *Dictyostelium* RasG, RasB, and RasD.[45] The data reported below was collected to monitor activation of these Ras proteins in response to cAMP stimulation. Since Ras is known to be activated at the leading edge of wild-type cells in a chemoattractant gradient,[45] the same uniform stimulation assay described previously was used to investigate this response.

3.5.2 Results

In AX3 cells, Ras activation peaks at roughly 5 seconds as indicated by membrane-localized RBD-GFP (Figure 6.4.A). Localization then returns to basal levels by approximately 30 seconds after stimulation and can again be seen localizing at membrane protrusions toward the end of the time lapse series (see final panel, T=57 secs, in Figure 6.4.A). When compared to

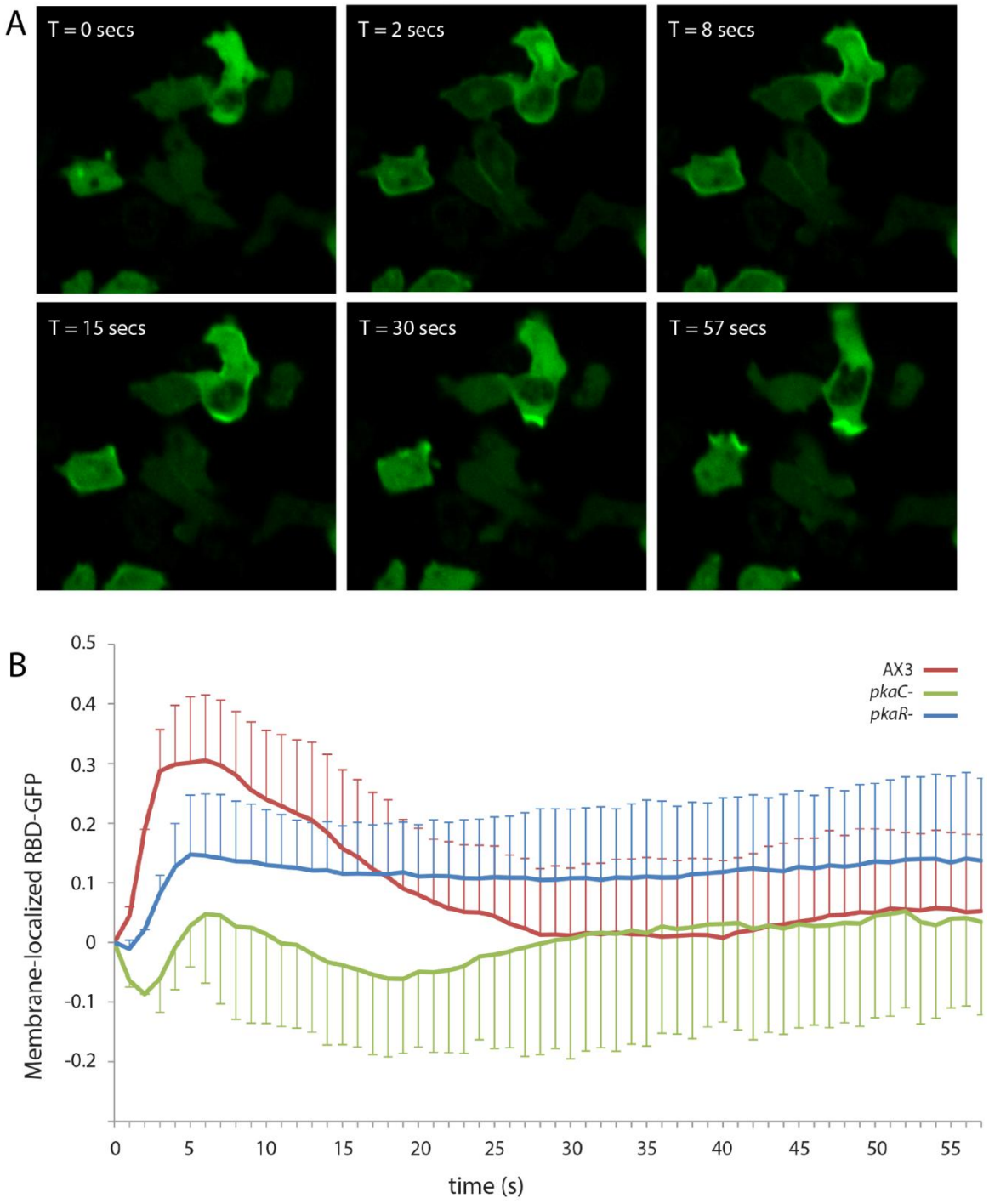

Figure 3.13.A. Response of AX3 cells containing GFP-RBD to uniform cAMP stimulation. Localization of the reporter at the membrane peaks at 5 seconds after stimulation of starved cells with cAMP. **B.** Relative to AX3 cells, both PKA mutants take slightly longer to respond to the stimulus and also display reduced levels of Ras activation. Sample sizes: AX3, 20 samples; *pkaC-*, 9 samples; *pkaR-*, 32 samples.

wild-type cells, *pkaR*- cells also exhibit a response to the cAMP stimulation, albeit at a lower magnitude. The most significant difference, however, is an apparent failure of these cells to return to their basal levels of membrane-localized RBD-GFP. In *pkaC*- cells, an interesting response is observed whereby the levels of membrane-localized RBD-GFP actually drop immediately following uniform stimulation instead of rapidly increasing. After this initial decrease, RBD-GFP returns to near-basal levels before decreasing once more.

3.5.3 Discussion

Only a few repetitions of this experiment were performed before other experiments took precedence. Fewer than 40 samples were compiled from each cell type to produce the graph in Figure 6.4.B., so more data needs to be collected in order to minimize error bars and confirm these trends. However, these preliminary findings seem to suggest possibly significant defects in Ras activation when PKA is either constitutively active or absent.

There are no known reporters for RasC, so we cannot probe its activity directly. However, as mentioned in the introduction, the RBD-GFP reporter is known to bind to RasG, RasB, and RasD; we base our conclusions about RasC activation on the knowledge that active RasC colocalizes with other Ras proteins at the plasma membrane of cAMP-stimulated cells.[15] We also know from biochemical activity assays (unpublished data) that RasC activation is lowered in *pkaC*- cells, providing further support for our hypothesis that PKA either directly or indirectly regulates Ras activity via feedback. This is particularly interesting as previously published studies show that cells lacking RasGAP NF1 have a phenotype very similar to that of the PKA null cells studied here.[46]

Considering evidence that TORC2 integrates signals from both RasC and Rap1 to control chemotaxis (see Introduction), we are also interested in looking at spatiotemporal activity of Rap1 in PKA mutant cell types. The experiment above confirms that there is misregulation of RasC activation in both *pkaC*- and *pkaR*- cells. Additional experiments include examination of Rap1 activation and localization in these same cell lines; this can be accomplished by using RalGDS-GFP,[47] a Ras-binding domain reporter for activated Rap1 which has been received and sequenced in anticipation of these experiments.

3.6 Rap1 Phosphorylation Mutants

As mentioned previously, Rap1 is a protein of particular interest in the signaling cascade controlling chemotaxis. Thus, we are also interested in investigating its upstream effectors. RapGAP1 is one phospho-protein that has been identified as a regulator of Rap1 activity and signaling.[48] Interestingly, whole-cell phosphoproteomics experiments (Charest, preliminary data) reveal PKA as one possible kinase that may be responsible for phosphorylating and, thus, regulating RapGAP1. Recent studies also identify potential PKA phosphorylation sites on RapGAP1.[49] However, it is also possible that PKA may directly phosphorylate Rap1, as recently reported in a study performed with mammalian cells.[50]

To ascertain the mechanism of Rap1 inhibition by PKA, experiments are planned to elucidate whether this regulation is direct or indirect through RapGAP1 or some other intermediate. Toward this end, both phosphomutant and phosphomimetic versions of Rap1 have been produced for use as controls. The phosphomutant, S181A, is a mutation of an alleged PKA phosphorylation site (serine 181) that renders it incapable of phosphorylation. As

its name implies, the phosphomimetic point mutation (S181E) mimics phosphorylation at this residue. These point mutations were introduced using site-directed mutagenesis (see Materials and Methods, Section 2.6.6). Mutations have been confirmed by sequencing and the DNA constructs will be utilized for future experiments.

Chapter 4. Conclusions and Future Directions

The work presented in this thesis advances understanding of the role of PKA in regulating polarization and chemotaxis. The chemotaxis phenotypes of pkaC- and pkaR- cells were investigated and compared to the wild-type (AX3) phenotype. It has been determined that both F-actin and Myosin II are spatially and temporally misregulated in both mutant cell lines, contributing to the polarization and migration defects observed in these cells.

PKA is a ubiquitous protein that likely affects a host of other signaling pathways when misregulated as it is in our PKA mutants. This may very likely be an explanation for the chemotaxis defects we observe, particularly in *pkaC*- cells where PKA activity entirely absent. Clearly these cells are viable, but it would be difficult to determine all of the widespread impacts of this mutation on other pathways that may play a role in mechanics of cell translocation. It is entirely possibly that PKA has more deleterious effects on other cytoskeletal proteins such as tubulin and microtubules which produce the phenotypes we observe.

Regardless, it certainly appears that there are effects on other components of the chemotaxis signaling cascade as evidenced by the biochemical assays performed thus far. There are two major known pathways that regulate F-actin: the GbpD-Rap1-Phg2 pathway and the RasG-PI3K pathway (Figure 7.1). We know that Rap1 regulates adhesion, cell polarity, and formation of pseudopods in Dictyostelium; considering our observations that Rap activity is affected in PKA null cells, it is very likely that this misregulation may explain the chemotaxis defects we observe.[40,51,52] Further experimentation is required to probe the nature of PKA-mediated Rap1 modulation—specifically, whether this regulations occurs directly or indirectly.

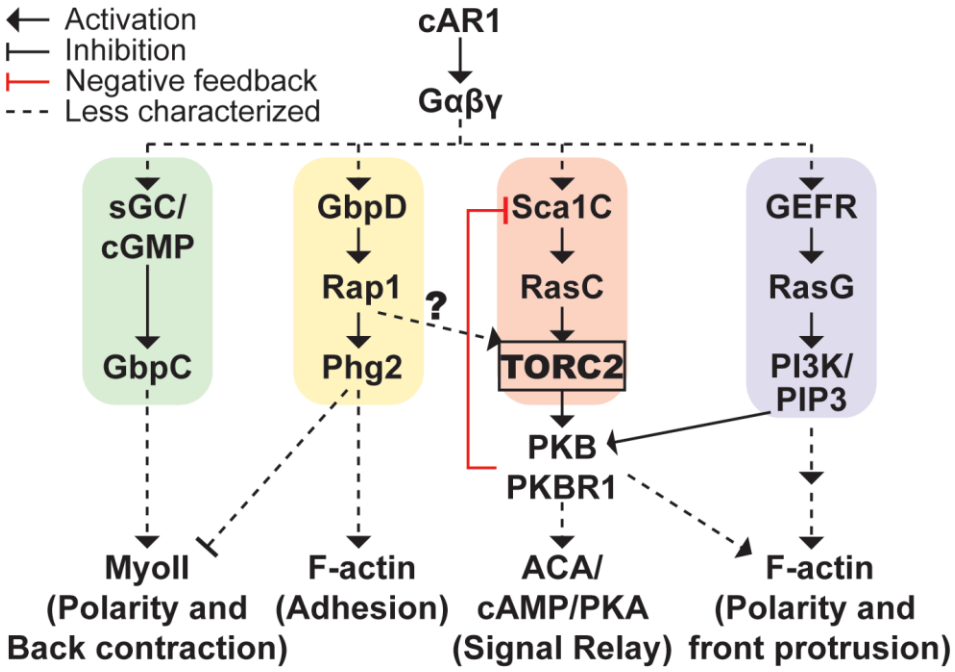

Figure 4.1. Key pathways implicated in chemoattractant signal transduction in Dictyostelium. The chemoattractant (cAMP) receptor cAR1 and downstream heterotrimeric G protein promote the activation of many downstream signaling pathways, in which Ras family GTPases play a central role. Further work needs to be done to address the potential cross-talk of RasC and Rap1 pathways through TORC2. (courtesy of Pascale Charest)

Similarly, we've observed that the RasG-PI3K pathway is misregulated, as evidenced by RBD-GFP studies (Section 6.2). This requires additional study, including imaging-based assays to survey localization of RBD-GFP during chemotaxis in all 3 cell lines (as described in the F-actin and Myosin II experiments). Since we know that the RasG-PI3K pathway controls F-actin polymerization,[53] misregulation here could also explain the actin localization defects we observe in the PKA null cell lines.

Future experiments include phenotypic analysis of cells treated with a peptide derived from the PKA inhibitor PKI (PKIpep) that binds to and inhibits PKA-C in mammals and *Dictyostelium*.[20,54–58] Spatiotemporal regulation of the cytoskeleton and GTPases in PKIpep-treated cells will also be investigated to compare their behavior to that of *pkaC*- cells, which have been shown to lack ACA and have gene expression defects.[59,60]

Additionally, a collaboration has been established to mathematically model the possible feedback loops based on the experimental data collected. In particular, this modeling will investigate the possibility that Rap1 and RasC work in parallel to regulate TORC2.

References

(1) Shaw, T. J.; Martin, P. Wound Repair at a Glance. *J. Cell Sci.* **2009**, *122*, 3209–3213.

(2) Ilina, O.; Friedl, P. Mechanisms of Collective Cell Migration at a Glance. *J. Cell Sci.* **2009**, *122*, 3203–3208.

(3) Woodfin, A.; Voisin, M. B.; Nourshargh, S. Recent Developments and Complexities in Neutrophil Transmigration. *Curr. Opin. Hematol.* **2010**, *17*, 9–17.

(4) Kedrin, D.; van Rheenen, J.; Hernandez, L.; Condeelis, J.; Segall, J. E. Cell Motility and Cytoskeletal Regulation in Invasion and Metastasis. *J. Mammary Gland Biol. Neoplasia* **2007**, *12*, 143–152.

(5) Richardson, B. E.; Lehmann, R. Mechanisms Guiding Primordial Germ Cell Migration: Strategies from Different Organisms. *Nat. Rev. Mol. Cell Biol.* **2010**, *11*, 37–49.

(6) Mortimer, D.; Fothergill, T.; Pujic, Z.; Richards, L. J.; Goodhill, G. J. Growth Cone Chemotaxis. *Trends Neurosci.* **2008**, *31*, 90–98.

(7) Friedl, P.; Weigelin, B. Interstitial Leukocyte Migration and Immune Function. *Nat. Immunol.* **2008**, *9*, 960–969.

(8) Lammermann, T.; Sixt, M. Mechanical Modes of “Amoeboid” Cell Migration. *Curr. Opin. Cell Biol.* **2009**, *21*, 636–644.

(9) Weiger, M. C.; Parent, C. A. Phosphoinositides in Chemotaxis. *Subcell. Biochem.* **2012**, *59*, 217–254.

(10) Wang, Y.; Chen, C.-L.; Iijima, M. Signaling Mechanisms for Chemotaxis. *Dev. Growth Differ.* **2011**, *53*, 495–502.

(11) Schaap, P. Evolutionary Crossroads in Developmental Biology: Dictyostelium Discoideum. *Development* **2011**, *138*, 387–396.

(12) Williams, J. G. Dictyostelium Finds New Roles to Model. *Genetics* **2010**, *185*, 717–726.

(13) Garcia, G. L.; Parent, C. a. Signal Relay during Chemotaxis. *J. Microsc.* **2008**, *231*, 529–534.

(14) Saran, S.; Meima, M. E.; Alvarez-Curto, E.; Weening, K. E.; Rozen, D. E.; Schaap, P. cAMP Signaling in Dictyostelium. Complexity of cAMP Synthesis, Degradation and Detection. *J. Muscle Res. Cell Motil.* **2002**, *23*, 793–802.

(15) Sasaki, A. T.; Firtel, R. A. Regulation of Chemotaxis by the Orchestrated Activation of Ras, PI3K, and TOR. *Eur. J. Cell Biol.* **2006**, *85*, 873–895.

(16) Loomis, W. F. Role of PKA in the Timing of Developmental Events in Dictyostelium Cells. *Microbiol. Mol. Biol. Rev.* **1998**, *62*, 684–694.

(17) Das, S.; Rericha, E. C.; Bagorda, A.; Parent, C. a. Direct Biochemical Measurements of Signal Relay during Dictyostelium Development. *J. Biol. Chem.* **2011**, *286*, 38649–38658.

(18) Lusche, D. F.; Bezares-Roder, K.; Happle, K.; Schlatterer, C. cAMP Controls Cytosolic Ca2+ Levels in Dictyostelium Discoideum. *BMC Cell Biol.* **2005**, *6*, 12.

(19) Maeda, M.; Lu, S.; Shaulsky, G.; Miyazaki, Y. Periodic Signaling Controlled by an Oscillatory Circuit That Includes Protein Kinases ERK2 and PKA. *Science* **2004**, *304*, 875–878.

(20) Simon, M. N.; Pelegrini, O.; Veron, M.; Kay, R. R. Mutation of Protein Kinase A Causes Heterochronic Development of Dictyostelium. *Nature* **1992**, *356*, 171–172.

(21) Loomis Jr, W. F. Sensitivity of Dictyostelium Discoideum to Nucleic Acid Analogues. *Exp. Cell Res.* **1971**, *64*, 484–486.

(22) Sussman, R.; Sussman, M. Cultivation of Dictyostelium Discoideum in Axenic Medium. *Biochem. Biophys. Res. Commun.* **1967**, *29*, 53–55.

(23) Cocucci, S. M.; Sussman, M. RNA in Cytoplasmic and Nuclear Fractions of Cellular Slime Mold Amebas. *J. Cell Biol.* **1970**, *45*, 399–407.

(24) Veltman, D. M.; Akar, G.; Bosgraaf, L.; Van Haastert, P. J. M. A New Set of Small, Extrachromosomal Expression Vectors for Dictyostelium Discoideum. *Plasmid* **2009**, *61*, 110–118.

(25) Fey, P.; Dodson, R. J.; Basu, S.; Chisholm, R. L. One Stop Shop for Everything Dictyostelium: dictyBase and the Dicty Stock Center in 2012. *Methods Mol. Biol.* **2013**, *983*, 59–92.

(26) Dynes, J. L.; Clark, A. M.; Shaulsky, G.; Kuspa, A.; Loomis, W. F.; Firtel, R. A. LagC Is Required for Cell-Cell Interactions That Are Essential for Cell-Type Differentiation in Dictyostelium. *Genes Dev.* **1994**, *8*, 948–958.

(27) Meima, M. E.; Weening, K. E.; Schaap, P. Vectors for Expression of Proteins with Single or Combinatorial Fluorescent Protein and Tandem Affinity Purification Tags in Dictyostelium. *Protein Expr. Purif.* **2007**, *53*, 283–288.

(28) Stochaj, W. R.; Berkelman, T.; Laird, N. Staining Membrane-Bound Proteins with Coomassie Blue r250. *CSH Protoc.* **2006**, *2006*.

(29) Zhang, H.; Heid, P. J.; Wessels, D.; Daniels, K. J.; Pham, T.; Loomis, W. F.; Soll, D. R. Constitutively Active Protein Kinase A Disrupts Motility and Chemotaxis in Dictyostelium Discoideum. *Eukaryot. Cell* **2003**, *2*, 62–75.

(30) Han, Y.-H.; Chung, C. Y.; Wessels, D.; Stephens, S.; Titus, M. A.; Soll, D. R.; Firtel, R. A. Requirement of a Vasodilator-Stimulated Phosphoprotein Family Member for Cell Adhesion, the Formation of Filopodia, and Chemotaxis in Dictyostelium. *J. Biol. Chem.* **2002**, *277*, 49877–49887.

(31) Jung, G.; Wu, X.; Hammer, J. A. Dictyostelium Mutants Lacking Multiple Classic Myosin I Isoforms Reveal Combinations of Shared and Distinct Functions. *J. Cell Biol.* **1996**, *133*, 305–323.

(32) Bosgraaf, L.; Russcher, H.; Smith, J. L.; Wessels, D.; Soll, D. R.; Van Haastert, P. J. M. A Novel cGMP Signalling Pathway Mediating Myosin Phosphorylation and Chemotaxis in Dictyostelium. *EMBO J.* **2002**, *21*, 4560–4570.

(33) Mendoza, M. C.; Du, F.; Iranfar, N.; Tang, N.; Ma, H.; Loomis, W. F.; Firtel, R. A. Loss of SMEK, a Novel, Conserved Protein, Suppresses MEK1 Null Cell Polarity, Chemotaxis, and Gene Expression Defects. *Mol. Cell. Biol.* **2005**, *25*, 7839–7853.

(34) Fey, P.; Kowal, A. S.; Gaudet, P.; Pilcher, K. E.; Chisholm, R. L. Protocols for Growth and Development of Dictyostelium Discoideum. *Nat. Protoc.* **2007**, *2*, 1307–1316.

(35) Insall, R. H.; Borleis, J.; Devreotes, P. N. The Aimless RasGEF Is Required for Processing of Chemotactic Signals through G-Protein-Coupled Receptors in Dictyostelium. *Curr. Biol.* **1996**, *6*, 719–729.

(36) Loovers, H. M.; Postma, M.; Keizer-Gunnink, I.; Huang, Y. E.; Devreotes, P. N.; van Haastert, P. J. Distinct Roles of PI(3,4,5)P3 during Chemoattractant Signaling in Dictyostelium: A Quantitative in Vivo Analysis by Inhibition of PI3-Kinase. *Mol. Biol. Cell* **2006**, *17*, 1503–1513.

(37) Sawai, S.; Thomason, P. A.; Cox, E. C. An Autoregulatory Circuit for Long-Range Self-Organization in Dictyostelium Cell Populations. *Nature* **2005**, *433*, 323–326.

(38) Riedl, J.; Crevenna, A.; Kessenbrock, K. Lifeact: A Versatile Marker to Visualize F-Actin. *Nature Methods* **2008**, *5*, 605–607.

(39) Lemieux, M. G.; Janzen, D.; Hwang, R.; Roldan, J.; Jarchum, I.; Knecht, D. A. Visualization of the Actin Cytoskeleton: Different F-Actin-Binding Probes Tell Different Stories. *Cytoskeleton (Hoboken).* **2013**, *00*, 1–13.

(40) Jeon, T. J.; Lee, D.-J.; Merlot, S.; Weeks, G.; Firtel, R. A. Rap1 Controls Cell Adhesion and Cell Motility through the Regulation of Myosin II. *J. Cell Biol.* **2007**, *176*, 1021–1033.

(41) Iwadate, Y.; Yumura, S. Actin-Based Propulsive Forces and Myosin-II-Based Contractile Forces in Migrating Dictyostelium Cells. *J. Cell Sci.* **2008**, *121*, 1314–1324.

(42) Moores, S. L.; Sabry, J. H.; Spudich, J. A. Myosin Dynamics in Live Dictyostelium Cells. *Proc. Natl. Acad. Sci. U S A* **1996**, *93*, 443–446.

(43) Alberts, B.; Johnson, A.; Lewis, J, et al. The Cytoskeleton and Cell Behavior. In *Molecular Biology of the Cell*; Garland Science: New York, 2002.

(44) Kae, H.; Lim, C.; Spiegelman, G.; Weeks, G. Chemoattractant-induced Ras Activation during Dictyostelium Aggregation. *EMBO Rep.* **2004**, *5*, 602–606.

(45) Sasaki, A. T.; Chun, C.; Takeda, K.; Firtel, R. A. Localized Ras Signaling at the Leading Edge Regulates PI3K, Cell Polarity, and Directional Cell Movement. *J. Cell Biol.* **2004**, *167*, 505–518.

(46) Zhang, S.; Charest, P. G.; Firtel, R. A. Spatiotemporal Regulation of Ras Activity Provides Directional Sensing. *Curr. Biol.* **2008**, *18*, 1587–1593.

(47) Kang, R. Evidence for a Role for the Dictyostelium Rap1 in Cell Viability and the Response to Osmotic Stress. *J. Cell Sci.* **2002**, *115*, 3675–3682.

(48) Jeon, T. J.; Lee, D.-J.; Lee, S.; Weeks, G.; Firtel, R. A. Regulation of Rap1 Activity by RapGAP1 Controls Cell Adhesion at the Front of Chemotaxing Cells. *J. Cell Biol.* **2007**, *179*, 833–843.

(49) McAvoy, T.; Zhou, M. M.; Greengard, P.; Nairn, A. C. Phosphorylation of Rap1GAP, a Striatally Enriched Protein, by Protein Kinase A Controls Rap1 Activity and Dendritic Spine Morphology. *Proc .Natl. Acad. Sci. U S A* **2009**, *106*, 3531–3536.

(50) Takahashi, M.; Dillon, T.; Liu, C.; Kariya, Y. Protein Kinase A-Dependent Phosphorylation of Rap1 Regulates Its Membrane Localization and Cell Migration. *J. Biol. Chem.* **2013**, *288*, 27712–27723.

(51) Kortholt, A.; Rehmann, H.; Kae, H.; Bosgraaf, L.; Keizer-Gunnink, I.; Weeks, G.; Wittinghofer, A.; Van Haastert, P. J. M. Characterization of the GbpD-Activated Rap1 Pathway Regulating Adhesion and Cell Polarity in Dictyostelium Discoideum. *J. Biol. Chem.* **2006**, *281*, 23367–23376.

(52) Kortholt, A.; Bolourani, P. A Rap/phosphatidylinositol 3-Kinase Pathway Controls Pseudopod Formation. *Mol. Biol. Cell* **2010**, *21*, 936–945.

(53) Kay, R. R.; Langridge, P.; Traynor, D.; Hoeller, O. Changing Directions in the Study of Chemotaxis. *Nat. Rev. Mol. Cell Biol.* **2008**, *9*, 455–463.

(54) Ashby, C. D.; Walsh, D. A. Characterization of the Interaction of a Protein Inhibitor with Adenosine 3’,5'-Monophosphate-Dependent Protein Kinases. II. Mechanism of Action with the Holoenzyme. *J. Biol. Chem.* **1973**, *248*, 1255–1261.

(55) Van Patten, S. M.; Ng, D. C.; Th’ng, J. P.; Angelos, K. L.; Smith, A. J.; Walsh, D. A. Molecular Cloning of a Rat Testis Form of the Inhibitor Protein of cAMP-Dependent Protein Kinase. *Proc. Natl. Acad. Sci. U S A* **1991**, *88*, 5383–5387.

(56) Mann, S. K.; Yonemoto, W. M.; Taylor, S. S.; Firtel, R. A. DdPK3, Which Plays Essential Roles during Dictyostelium Development, Encodes the Catalytic Subunit of cAMP-Dependent Protein Kinase. *Proc. Natl. Acad. Sci. U S A* **1992**, *89*, 10701–10705.

(57) Thomason, P. A.; Traynor, D.; Cavet, G.; Chang, W. T.; Harwood, A. J.; Kay, R. R. An Intersection of the cAMP/PKA and Two-Component Signal Transduction Systems in Dictyostelium. *EMBO J* **1998**, *17*, 2838–2845.

(58) Ryves, W. J.; Harwood, A. J. Use of a Penetratin-Linked Peptide in Dictyostelium. *Mol. Biotechnol.* **2006**, *33*, 123–132.

(59) Mann, S. K.; Brown, J. M.; Briscoe, C.; Parent, C.; Pitt, G.; Devreotes, P. N.; Firtel, R. A. Role of cAMP-Dependent Protein Kinase in Controlling Aggregation and Postaggregative Development in Dictyostelium. *Dev. Biol.* **1997**, *183*, 208–221.

(60) Harwood, A. J.; Hopper, N. A.; Simon, M.-N.; Bouzid, S.; Veron, M.; Williams, J. G. Multiple Roles for cAMP-Dependent Protein Kinase during Dictyostelium Development. *Dev. Biol.* **1992**, *149*, 90–99.